

1 **THE CARRANCAS FORMATION, BAMBUÍ GROUP: A RECORD OF PRE-MARINOAN**  
2 **SEDIMENTATION ON THE SOUTHERN SAO FRANCISCO CRATON, BRAZIL**

3 Gabriel J. Uhlein<sup>1,3\*</sup>; Alexandre Uhlein<sup>1</sup>; Galen P. Halverson<sup>2</sup>; Ross Stevenson<sup>3</sup>; Fabrício A. Caxito<sup>1</sup>;  
4 Grant M. Cox<sup>2</sup>; Jorge F.M.G. Carvalho<sup>4</sup>

5  
6 1 – Centro de Pesquisas Manoel Teixeira da Costa, Instituto de Geociências, Universidade Federal de Minas Gerais,  
7 Campus Pampulha, Av. Antônio Carlos 6627, 31270-901, Belo Horizonte, MG, Brazil - \*corresponding author:  
8 [guhlein@gmail.com](mailto:guhlein@gmail.com);

9 2 - Department of Earth and Planetary Sciences/GEOTOP, McGill University, Montréal, Québec H3A 0E8, Canada

10 3 - GEOTOP, Université du Québec à Montréal, P.O. Box 8888, Station Centre Ville, Montreal, Quebec H3C 3P8,  
11 Canada

12 4 – Petrobras S.A., Av. Nossa Senhora da Penha, 1688, 29057-570, Vitória, ES, Brazil.

13

14 **ABSTRACT**

15 The Carrancas Formation outcrops in east-central Brazil on the southern margin of São  
16 Francisco craton where it comprises the base of the late Neoproterozoic Bambuí Group. It is overlain  
17 by the basal Ediacaran cap carbonate Sete Lagoas Formation and was for a long time considered to  
18 be glacially influenced and correlative with the glaciogenic Jequitaí Formation. New stratigraphic,  
19 isotopic and geochronologic data imply that the Carrancas Formation was instead formed by the  
20 shedding of debris from basement highs uplifted during an episode of minor continental rifting.  
21 Reddish dolostones in the upper Carrancas Formation have  $\delta^{13}\text{C}$  values ranging from +7.1 to +9.6‰,  
22 which is a unique C isotopic composition for the lowermost Bambuí Group but similar to values  
23 found in the Tijucuçu sequence, a pre-glacial unit in the Araçuaí fold belt on the eastern margin of  
24 the São Francisco craton. The stratigraphic position below basal Ediacaran cap carbonates and the  
25 highly positive  $\delta^{13}\text{C}$  values together imply a Cryogenian interglacial age for the Carrancas  
26 Formation, with the high  $\delta^{13}\text{C}$  values representing the so-Keele peak, which precedes the pre-  
27 Marinoan Trezona negative  $\delta^{13}\text{C}$  excursion in other well characterized Cryogenian sequences.  
28 Hence, The Carrancas Formation pre-dates de Marinoan Jequitaí Formation and represents an  
29 interval of Cryogenian stratigraphy not previously known to occur on the São Francisco craton.  
30 Documentation of Cryogenian interglacial strata on the São Francisco craton reinforces recent  
31 revisions to the age of Bambuí Group strata and has implications for the development of the Bambuí  
32 basin.

33

1 Keywords: Neoproterozoic; Marinoan glaciation; isotope stratigraphy; Keele peak; São  
2 Francisco craton; Bambuí Group.

### 3 1. INTRODUCTION

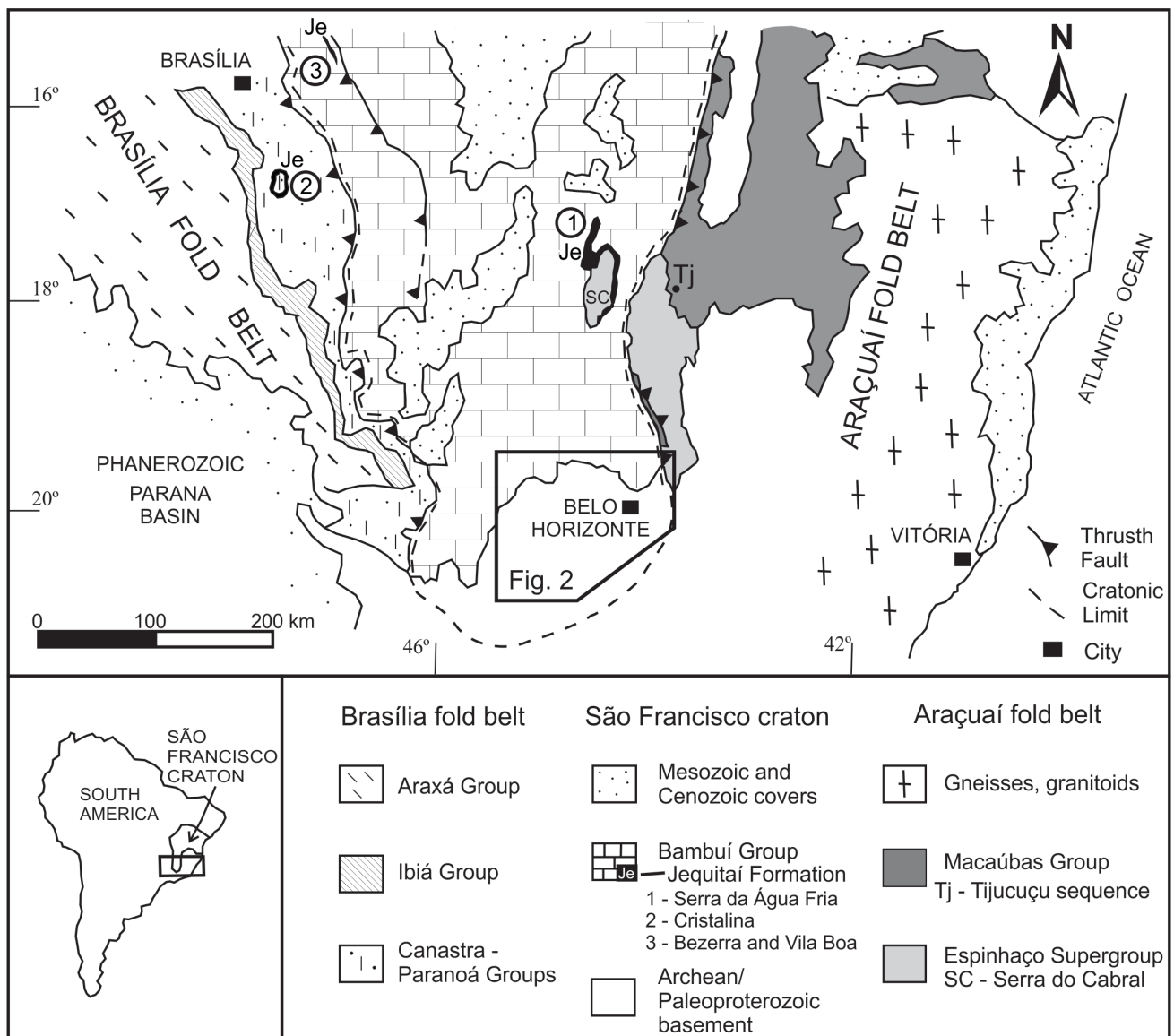
4 The end-Cryogenian glaciation (i.e. ca. 635 Marinoan event) left a unique imprint in the  
5 geological record in the form of lithologically and geochemically distinctive carbonates that were  
6 deposited globally during the post-glacial transgression (e.g.: Halverson *et al.*, 2004; Allen and  
7 Hoffman, 2005; Shields, 2005; Hoffman *et al.*, 2007). The sedimentary processes operating during  
8 this transgression remain controversial (e.g. James *et al.*, 2001; Lamb *et al.* 2012), in particular with  
9 regards to the transition from glacially-related siliciclastics to deposition of carbonates typically  
10 associated with a tropical climate (Allen and Hoffman, 2005; Eyles and Januszczak, 2004; Font *et*  
11 *al.*, 2010; Hoffman *et al.*, 2007; Hoffman, 2011; Kennedy and Christie-Blick, 2011). Paleomagnetic  
12 and other paleogeographic constraints suggest that this glaciation occurred on a planet with sparse or  
13 no high latitude continents (Evans, 2000; Trindade and Macouin, 2007; Hoffman and Li, 2009).

14 A better understanding of this pivotal transition in Earth's history can be gleaned from  
15 integrated sedimentological, geochemical, geochronological and isotopic studies of the many  
16 Neoproterozoic siliciclastic-carbonate successions that were deposited at this time as the  
17 supercontinent Rodinia broke up. Despite a growing body of data and renewed interest in the late  
18 Neoproterozoic Bambuí Group on the southern margin of the São Francisco craton (east-central  
19 Brazil), considerable debate persists over the age and origin of the Bambuí basin (Fig. 1). While it  
20 had long been thought that the Jequitaí Formation and overlying lower Sete Lagoas Formation in the  
21 lower Bambuí Fm. represent the older Cryogenian (Sturtian) glaciation and its overlying cap  
22 carbonate sequence, respectively (e.g. Babinsky *et al.* 2007; Vieira *et al.*, 2007b), more recently, other  
23 authors have advocated that they are late Cryogenian–Ediacaran in age, based on a combination of  
24 sedimentological and isotopic characteristics (Caxito *et al.*, 2012; Alvarenga *et al.*, 2014). However,  
25 this significant chronostratigraphic revision to the lower Bambuí Group is complicated by the recent  
26 discovery of the distinctly late Ediacaran fossils *Cloudina* (Warren *et al.*, 2014) and ca. 550 Ma  
27 detrital zircons in the middle of the Sete Lagoas Formation (Paula-Santos *et al.*, 2015).

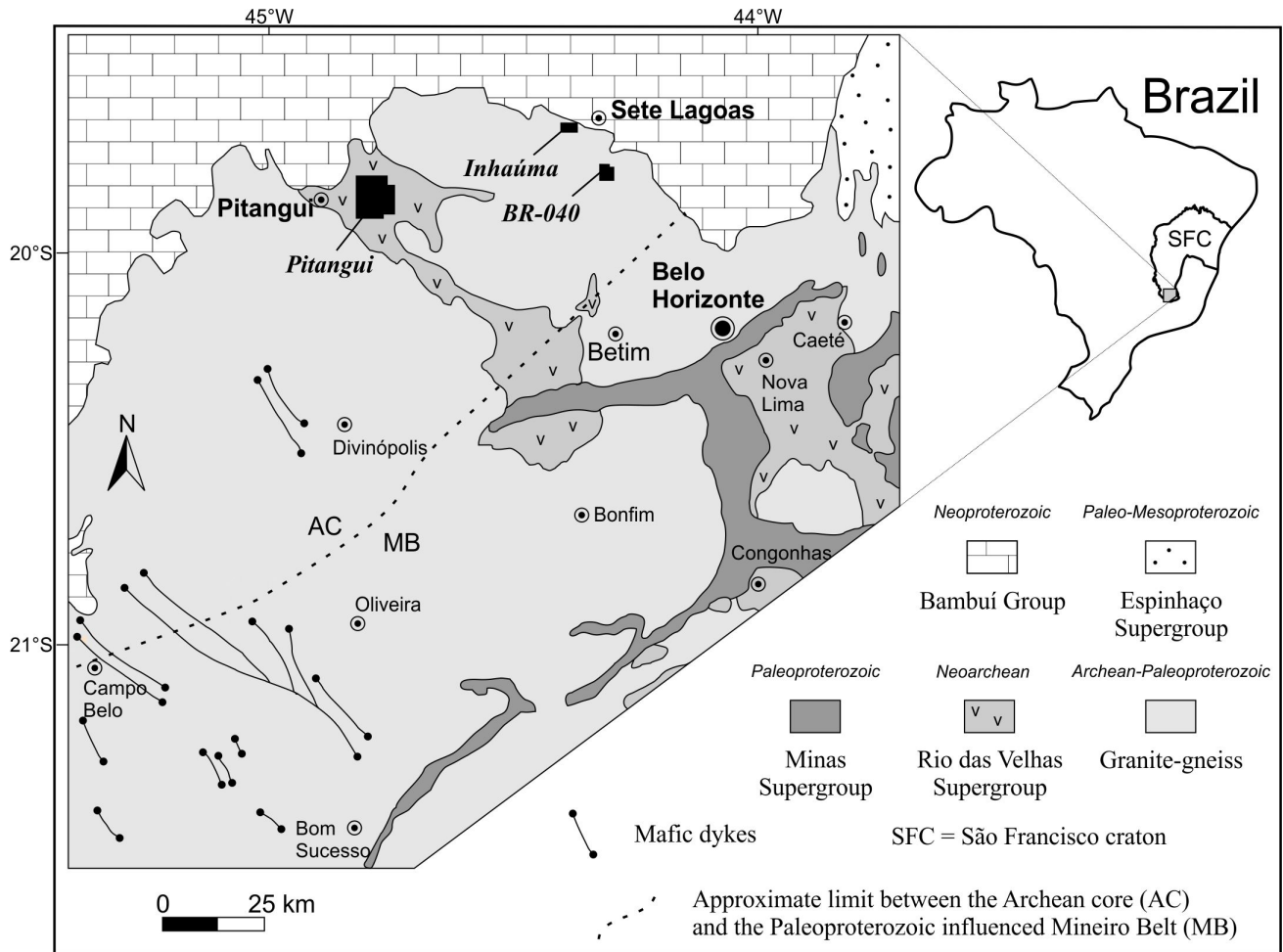
28 Additional debate surrounds the nature of the Carrancas Formation, which locally comprises  
29 the lower Bambuí Group (Fig. 2). The Carrancas Formation outcrops in basement lows, below the  
30 cap carbonates of the Sete Lagoas Formation and was long considered to be glaciogenic and  
31 correlated with the Jequitaí Formation. However, no unambiguous glacial evidence has been found

1 (e.g.: Martins-Neto *et al.*, 2001), and Caxito *et al.* (2012) argued that some facies of the Carrancas  
 2 Formation are represent reworked post-Marinoan cap carbonate and basement.

3 Here we present stratigraphic analysis and new whole-rock geochemistry, Nd isotopes, U-Pb  
 4 geochronology and C and O isotopes on carbonate clasts and layers from three outcrop areas of the  
 5 Carrancas Formation that clarify its depositional environment and tectonic context. The data imply  
 6 that the Carrancas Formation pre-dates the end-Cryogenian glaciation and records sedimentation in  
 7 basement lows during an episode of minor continental extension on the southern São Francisco  
 8 paleocontinent. These interpretations have major implications for the Neoproterozoic stratigraphy of  
 9 the São Francisco craton and surrounding fold belts and motivate a new model of the sedimentary  
 10 processes and paleogeography before the end-Cryogenian glaciation in southwest Gondwana.



1 Fig. 1: Simplified geologic map of the central and southern São Francisco craton and marginal fold  
 2 belts. The circled numbers show locations where the Jequitai Fm. occurs, and the location of the  
 3 Tijucuçu sequence is also shown. See Fig. 2 for detail of the region investigated for this project.  
 4 Geologic map after Almeida (1977), Alkmim and Marshak (1998) and Alkmim and Martins-Neto  
 5 (2001).



6  
 7 Fig. 2: Simplified geologic map of the southern São Francisco craton. Studied occurrence areas of  
 8 the Carrancas Formation in black polygons; see text for stratigraphic details. Modified from Teixeira  
 9 *et al.* (2000).

## 10 2. GEOLOGICAL SETTING

### 11 2.1. The Bambuí Group

12 The Bambuí Group is a late (< 635 Ma) Neoproterozoic mixed carbonate-siliciclastic sequence that  
 13 covers over 300,000 km<sup>2</sup> of the São Francisco craton in east-central Brazil (Fig. 1; Alkmim and  
 14 Martins-Neto, 2001; Sial *et al.*, 2009). Dardenne (1978) defined six formations, from base to top: (1)  
 15 Jequitai / Carrancas Formation — conglomerates, sandstones and shales; (2) Sete Lagoas Formation  
 16 — mainly carbonates; (3) Serra de Santa Helena Formation — siltstones, shales and rhythmites; (4)

1 Lagoa do Jacaré Formation — oolitic and intraformational carbonates; (5) Serra da Saudade  
2 Formation — siltstones, shales and sandstones; (6) Três Marias Formation — mainly sandstones.  
3 Recently, a lateral equivalent to the Serra da Saudade Formation was proposed in the western part of  
4 the basin: the Lagoa Formosa Formation, consisting of intraformational diamictite, siltstone,  
5 sandstone, and lenses of limestone and jaspilite (Sial *et al.*; 2009; Uhlein *et al.* 2011a). Although the  
6 Bambuí Group is commonly considered to be conformable, Santos *et al.* (2004), Zalán and Romeiro-  
7 Silva (2007) and Martins and Lemos (2007) interpreted a major unconformity in the middle of the  
8 Sete Lagoas Formation separating a lower sequence deposited in an intracratonic basin from an  
9 upper foreland sequence. This interpretation was largely based on seismic and regional  
10 chemostratigraphic ( $\delta^{13}\text{C}$ ) data; however, robust field evidence for the unconformity has not been  
11 documented yet.

12 The depositional age of the Bambuí Group is a topic of intense debate. Babinski *et al.* (2007)  
13 obtained a tight Pb-Pb isochron array of  $740\pm 20$  Ma on carbonates near the city of Sete Lagoas,  
14 indicating that the Sete Lagoas Formation was a middle-Cryogenian (i.e. Sturtian) cap carbonate.  
15 However, the Sete Lagoas does not resemble typical post-Sturtian cap carbonates, and Caxito *et al.*  
16 (2012) instead argued for a basal Ediacaran age, supported by lithostratigraphic features (e.g. basal  
17 cap dolomite and overlying seafloor cements), carbon and oxygen isotope profiles, and  $^{87}\text{Sr}/^{86}\text{Sr}$   
18 signatures that allied it with post-Marinoan cap carbonates globally.

19 More recent geochronological results from the Sete Lagoas Formation imply a potentially  
20 younger Ediacaran age. For example, detrital zircons from the Sete Lagoas Formation are as young  
21 as ca. 550 Ma, yielding a concordia age with the youngest grains of  $592\pm 1.7$  Ma (Paula-Santos *et al.*,  
22 2015). Warren *et al.* (2014) recovered *Cloudina* fragments from the middle Sete Lagoas Formation  
23 near the city of Januária, in the north of Minas Gerais state, also implying a late Ediacaran age for  
24 the middle part of this formation towards the top of the Bambuí Group. These authors argued for a  
25 marine link between South America, Africa, and probably Antarctica that would have provided the  
26 ideal conditions for the *Cloudina* occurrence on the São Francisco craton. In contrast, Paula-Santos  
27 *et al.* (2015) argued that the Bambuí basin was confined and restricted from the open ocean to  
28 account for the discrepancy between middle to late Ediacaran detrital zircon ages and persistent  
29  $^{87}\text{Sr}/^{86}\text{Sr}$  ratios of 0.7074-0.7076, which are typical of early Ediacaran rocks globally.

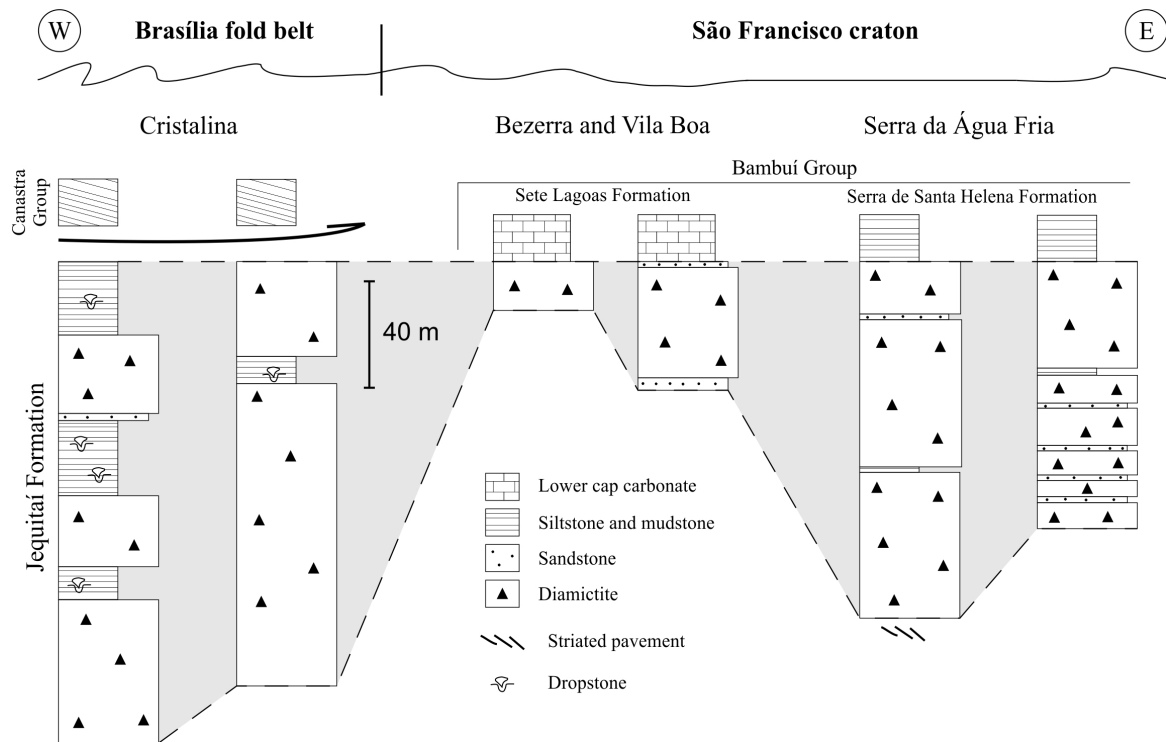
30 A middle-late Ediacaran age is also contradicted by K-Ar muscovite cooling ages of  $588\pm 15$   
31 and  $567\pm 17$  Ma on nappes of the Brasília fold belt, which were thrust over the southwestern margin  
32 of the Bambuí basin, implying that the Bambuí Group predates the middle Ediacaran (Valeriano *et al.*  
33 *et al.*, 2000). Similarly, on the eastern São Francisco craton, the minimum depositional age is well  
34 constrained between 590 and 545 Ma from zircon crystallization ages of the syn-collisional G2

1 granitic supersuite in the Araçuaí fold belt, which structurally affected the eastern margin of the  
2 Bambuí basin (e.g. Pedrosa-Soares *et al.*, 2001; Gonçalves *et al.*, 2015). It is evident that different  
3 datasets have yielded contradictory age constraints for the Bambuí Group, with very different  
4 implications for the evolution of the São Francisco craton and Ediacaran Earth history. Despite those  
5 complications, the emerging picture is one of deposition of the entire Bambuí Group from the Sete  
6 Lagoas upwards during the Ediacaran Period, perhaps terminating at around 540 Ma as suggested by  
7 the younger deformational ages of both the Brasília and Araçuaí fold belts.

## 8 **2.2. Jequitaiá Formation**

9 The Jequitaiá Formation outcrops in several regions, from the central São Francisco craton to  
10 the eastern margin of the Brasília fold belt (Fig. 1). At Serra da Água Fria, close to the Serra do  
11 Cabral, the Jequitaiá Formation locally comprises the base of the Bambuí Group and is widely  
12 recognized as being of glacial origin (e.g.: Isotta *et al.*, 1969; Uhlein *et al.*, 1999, 2011b; Cukrov *et*  
13 *al.*, 2005). The Jequitaiá Formation reaches thickness of >150 m and is predominantly composed of  
14 massive diamictites. Very rare and narrow centimetre- to metre-scale alternations of sandstones and  
15 pelites in the Serra da Água Fria contrast with thicker siltstones intercalations and pebble-sized  
16 dropstones of quartzites in the Cristalina region (Fig. 3). The diamictites contain granules to large  
17 boulders, which are angular to sub-rounded and composed of sandstones, carbonates, pelites, granites  
18 and gneisses, vein quartz and diverse volcanic rocks. Isotta *et al.* (1969) discovered a striated  
19 pavement on sandstones in the Serra da Água Fria region. Later, Rocha-Campos *et al.* (1996) re-  
20 interpreted the glacial abrasion to have formed over a soft substrate beneath a marine ice sheet,  
21 implying a foreshore depositional setting (Uhlein *et al.*, 1999, 2011b; Cukrov *et al.*, 2005; see also  
22 Caxito *et al.* 2012). In the Cristalina region, the greater thickness of the Jequitaiá Formation,  
23 occurrence of dropstones, and absence of striated pavements together imply a deep offshore  
24 environment (Cukrov *et al.*, 2005) (Fig. 3).

25 Other diamictite occurrences in the Bezerra and Vila Boa regions (Fig. 1 and 3), below cap  
26 carbonates of the Sete Lagoas Formation, are unambiguously correlated with the Jequitaiá Formation  
27 and suggest deposition in terminal moraines atop a basement of Mesoproterozoic Paranoá Group  
28 (Alvarenga *et al.*, 2007, 2014; Martins-Ferreira, 2013).



1

2 Fig. 3: Stratigraphic logs of the end-Cryogenian glaciogenic Jeiquitaí Formation plotted in a W-E  
 3 profile, from the Brasília fold belt to the undeformed São Francisco craton. The top of the Jeiquitaí  
 4 Formation is used as the datum. Stratigraphic data from Uhlein *et al.* (1999, 2011b); Cukrov *et al.*  
 5 (2005); Alvarenga *et al.* (2007); Martins-Ferreira *et al.* (2013); Alvarenga *et al.* (2014). See Fig. 1  
 6 for locations.

7

### 2.3. Carrancas Formation

8 The Carrancas Formation is a conglomerate-bearing unit patchily preserved at the base of the  
 9 Bambuí Group (Fig. 2). A type section of 20-30 meters of diamictites overlain by rhythmites and  
 10 overlain sharply by basal Ediacaran cap carbonates of the Sete Lagoas Formation was established by  
 11 Tuller *et al.* (2008) in the Inhaúma region for the Carrancas Formation.

12 The classic outcrop of the Carrancas Formation at the 30 km marker of the MG-424 road  
 13 consists of a 3 m-thick conglomerate with a sandy-calcareous matrix and pebble- to boulder-sized  
 14 clasts of gneiss, dolostone, limestone, granite and quartz. Caxito *et al.* (2012) suggested that the  
 15 calcite-rich matrix and the occurrence of carbonate clasts, with petrological and isotopic  
 16 characteristics identical to the lower Sete Lagoas Formation, are most consistent with a derivation  
 17 from local reworking of the basal carbonate platform, along with its basement. This interpretation  
 18 clearly distinguishes the Carrancas Formation from the Jeiquitaí Formation chronologically,  
 19 suggesting that it is a lateral equivalent of the cap carbonate that was formed by the shedding of cap  
 20 carbonate debris deposited during the post-glacial transgression deposition. However, recent road cut  
 21 exposures have revealed that the conglomerate at this classic outcrop sits atop a sharp contact with

1 lower Sete Lagoas Formation carbonates. The paraconglomerate actually shows a lenticular  
2 geometry, and it is bound below and above by carbonates of the Sete Lagoas Formation. Thus, it is  
3 clear that this outcrop is not correlative with the Carrancas Formation proper, which strictly lies  
4 below the Sete Lagoas Formation.

5 Although evidence for glacial influence on the Carrancas Formation is typically absent or  
6 equivocal, it was long considered to be glacial in origin (Martins-Neto *et al.*, 2001; Sgarbi *et al.*,  
7 2003; Romano and Knauer, 2003; Romano, 2007; Ribeiro *et al.*, 2008; Reis and Alkmim, 2015) and  
8 correlated with the Jequitai Formation, which occurs basin-wide. Indeed, recent synthesis of detailed  
9 stratigraphic and sedimentary data from the southern Bambuí basin showed no evidence of glacial  
10 activity in the Carrancas Formation, which is instead interpreted as having been deposited in  
11 basement lows along fault margins (Vieira *et al.*, 2007a,b; Uhlein *et al.*, 2013). However, a more  
12 thorough definition of the Carrancas Formation and interpretation of its significance with respect to  
13 the early stages of the Bambuí basin deposition and its timing relative to the end-Cryogenian  
14 glaciation are required.

### 15 3. SAMPLING AND ANALYTICAL PROCEDURES

16 Care was taken to select the freshest samples, with a preference for fine-grained lithologies  
17 for all geochemical analyses. Following removal of any weathered and veined surfaces, samples  
18 were crushed in a jaw crusher, and a fraction of the resulting fragments was then pulverized in a ball  
19 mill.

20 Trace and rare earth elements analyses were performed by ACME Analytical Laboratories  
21 Ltd. (Vancouver, Canada). Concentrations were measured via ICP-MS after fusion with lithium  
22 metaborate / tetraborate and digestion with diluted nitric acid. Analytical errors are within 5% for  
23 major and minor elements and 10–15% for trace elements. Loss on Ignition (LOI) was determined by  
24 weight loss after ignition at 1000°C.

25 The Sm-Nd isotope analyses were conducted in Radiogenic Isotope Laboratory at GEOTOP-  
26 UQÀM (Montréal, Canada). The samples were dissolved in an HF-HNO<sub>3</sub> mixture in Teflon vessels  
27 in which a <sup>150</sup>Nd-<sup>149</sup>Sm tracer was also added in order to determine Nd and Sm concentrations. Rare  
28 earth elements (REEs) were separated by cation exchange chromatography, and Sm and Nd were  
29 subsequently isolated following the procedure of Pin and Zalduegui (1997). The total procedural  
30 blanks are less than 150 pg. Sm and Nd analyses were performed using a double filament assembly  
31 on a Thermo Scientific Triton Plus mass spectrometer in static mode. The Sm and Nd concentrations  
32 and the <sup>147</sup>Sm/<sup>144</sup>Nd ratios have an accuracy of 0.5% that corresponds to an average error on the

1 initial  $\epsilon_{\text{Nd}}$  value of  $\pm 0.5$  epsilon units, based on repeated measurements of standards JNdi and  
2 BHVO-2.

3 Carbon and oxygen isotope ratios were measured on a Nu Perspective dual-inlet isotope ratio  
4 mass spectrometer connected to a NuCarb carbonate preparation system in the McGill University  
5 Stable Isotope Laboratory (Montréal, Canada). Approximately 100  $\mu\text{g}$  of sample powder was  
6 weighed into glass vials and reacted individually with  $\text{H}_3\text{PO}_4$  after heating to  $90^\circ\text{C}$  for 1 hour. The  
7 released  $\text{CO}_2$  was collected cryogenically and isotope ratios were measured against an in-house  
8 reference gas in dual inlet mode. Samples were calibrated to VPDB (Vienna Pee Dee Belemnite)  
9 using house standards. Errors better than 0.05‰ ( $1\sigma$ ) for both  $\delta^{13}\text{C}$  and  $\delta^{18}\text{O}$  based on repeat  
10 analyses of standards.

11 Zircon grains were analyzed at the Laboratório de Geocronologia, Universidade de Brasília,  
12 Brazil, by laser ablation on a Finnigan Neptune multi-collector ICP-MS coupled to a Nd-YAG 213  
13 nm laser ablation system. The U–Pb analyses follow the procedures outlined in Bühn *et al.* (2009).  
14 Ablation was carried out using 25–30  $\mu\text{m}$  spots in raster mode, at a frequency of 9–13 Hz and  
15 intensity of 0.19–1.02  $\text{J}/\text{cm}^2$ . The ablated material was carried by Ar ( $\sim 0.90$  L/min) and He ( $\sim 0.40$   
16 L/min) in 40 cycles of 1 s each, following a standard-sample bracketing of three sample analyses  
17 between a blank and a GJ-1 zircon standard. Accuracy was controlled using the TEMORA-2  
18 standard. Raw data was reduced using an in-house program and corrections were done for  
19 background, instrumental mass bias and common Pb. U–Pb ages were calculated using Isoplot 3.6  
20 (Ludwig, 2008).

## 21 4. RESULTS AND INTERPRETATIONS

22 The Carrancas Formation overlies Archean-Paleoproterozoic granite-gneiss of the Belo  
23 Horizonte Complex and Neoproterozoic meta-volcano-sedimentary rocks of the Rio das Velhas  
24 Supergroup. Both units are part of the uplifted cratonic basement that forms the Sete Lagoas paleo-  
25 high on the southern São Francisco Craton (e.g. Teixeira *et al.*, 2000; Alkmim, 2004) (Fig. 2). Here  
26 we summarize the stratigraphic, sedimentological, isotopic ( $\delta^{13}\text{C}$ ,  $\delta^{18}\text{O}$ ) and geochronological (Sm-  
27 Nd, U-Pb) records in the Carrancas Formation outcrop areas. Four facies associations are described  
28 from these areas (Table 1 and Fig. 2): clast- to matrix-supported conglomerates and breccias (FA1);  
29 coarse to fine-grained sandstone (FA2); mudstone and siltstone with black shale (FA3), and sandy-  
30 siltstone and dolostone (FA4).

### 31 4.1. Sedimentological and stratigraphic analyses of the Carrancas Formation

#### 4.1.1. Pitangui area

The Carrancas Formation in the Pitangui area overlaps metasedimentary rocks (mainly mica-schist and quartzite) of the Neoproterozoic Rio das Velhas Supergroup (Fig. 2) and is composed of clast-supported conglomerates, breccias and diamictites at the base (FA1) passing gradually upward to coarse- to fine-grained sandstones (FA2) (Fig. 4A and 5). The matrix consists of fine-sand to silty quartz, and the dominant clast lithologies derive from the local basement comprising the meta-volcano-sedimentary Rio das Velhas Supergroup: quartzite, granitoid, gneiss, schist, quartz pebbles and chert. Dolomite clasts from an unknown source are also present. Clasts range from small pebbles to large boulders in size and are angular to sub-rounded. Clast size and clast/matrix ratio gradually decrease toward the top until diamictite layers predominate. The diamictite contains small-pebbles of carbonate, quartzite, schist and chert, along with small (0.2 cm) limonitized pyrite scattered through a matrix composed by clay minerals and silt to fine-sand quartz.

Above and laterally conglomerates and diamictites, massive conglomeratic sandstones occur, with locally pebbles of quartz and schist. They are rarely intercalated with normal graded, fine-grained sandstones and with small-scale tabular cross-stratification. We interpret coarse-grained sedimentary rocks and sandstones to represent deposition on alluvial fan, from proximal to distal fan, respectively, likely as a result of local block faulting and basement uplift.

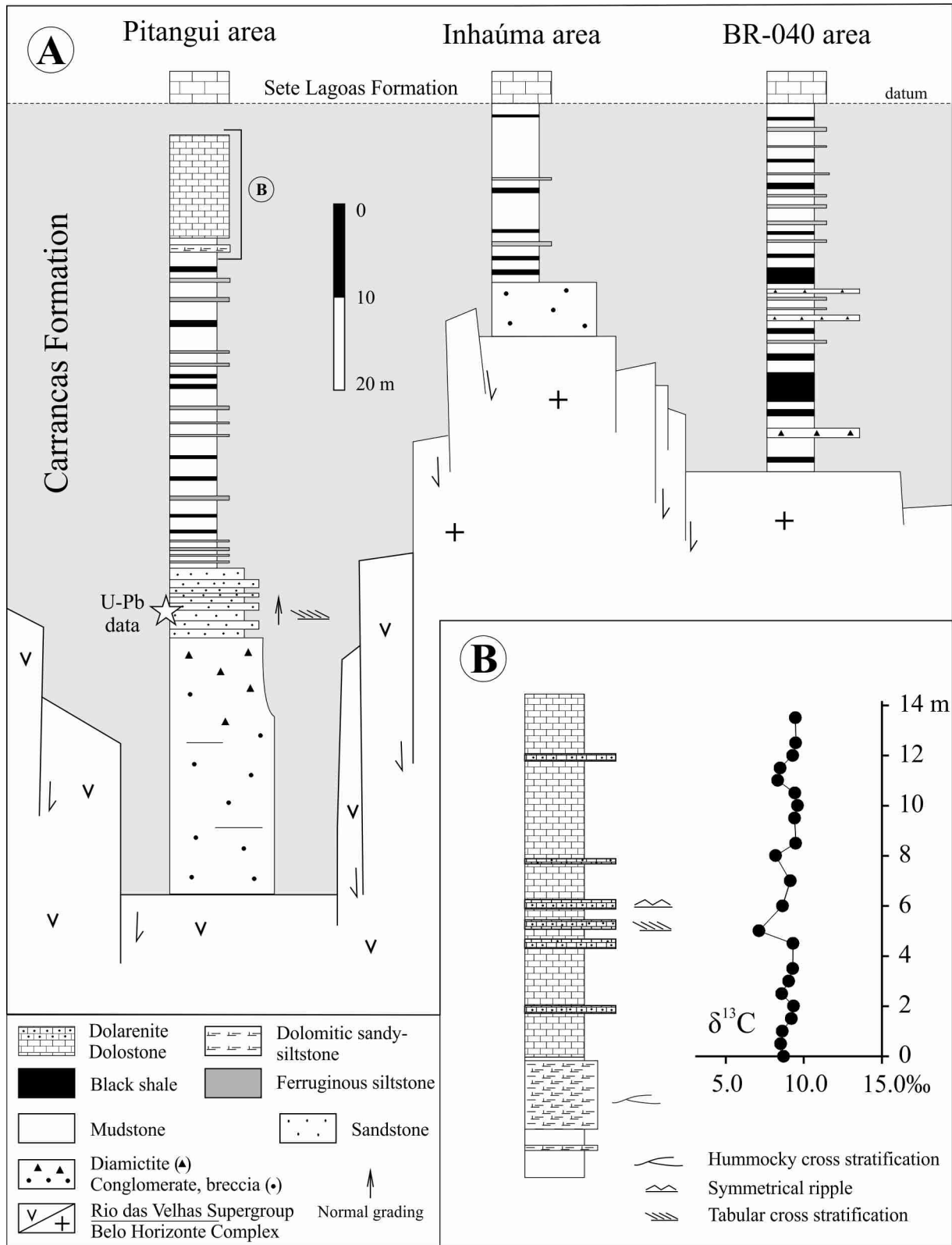
Mudstones, siltstones and rhythmites of FA3 (Table 1) variably overlie basement rocks, FA1 and FA2. Mudstones are interbedded with ferruginous siltstones and black shales, which have total organic contents (TOC) of up to 1.5% (Fig. 5). These facies commonly pass from ferruginous siltstones up into black shale, and mud-silt couplets (rhythmites) are commonly intercalated in with massive mudstones. These facies are widespread and common in all studied areas.

Upsection, a gradual increase in the abundance of sand-sized grains, eventually transitioning into sandy-siltstones beds, which also contain dolomitic grains. Bedded and laminated dolomitic sandy-siltstone with common hummocky cross-stratification occurs below an overlying transitional contact with reddish dolomites. Bedded and finely laminated reddish dolomite form a unit ~15 m thick locally show low-angle tabular cross-stratification and small-scale wave ripples (dolarenite), interbedded with thin (2-5 cm) beds of greenish siltstone (Fig. 4A, 4B and 5). The dolomitic sandy-siltstone with hummocky cross-stratification below dolomites with wave ripples suggest deposition in a shallower depositional setting influenced by tidal currents.

In the Pitangui area, the quartzites and metaconglomerates of the Rio das Velhas Supergroup outcrop at higher elevations, while the lithofacies of the Carrancas Formation are all limited to

- 1 topographic lows. The stratigraphy seems to track the present geography, with thicker intervals of the
- 2 clast-supported conglomerates, breccias and diamictites close to topographic highs.
- 3 Table 1: Facies associations of the Carrancas Formation in studied areas. See text for details and
- 4 occurrences in each area.

Facies association	Facies	Sedimentary structures	Other characteristics	Depositional setting	Processes
FA1	Cast-supported breccia	Massive, rarely layered	Sandy matrix. Granule to boulder in size clasts sampling local basement and from area to area. Locally carbonates intraclasts.	Alluvial fan	Debris/mud flows
	Clast-supported conglomerate	Massive			
	Diamictite	Massive	Mud-silt greenish matrix. Pebble-sized clasts of siltstone and carbonate		
FA2	Fine-grained sandstone	Layered; normally graded beds; tabular cross stratification	Greenish when fresh.	Distal alluvial fan; fan channels	Hyperconcentrated to normal stream flows.
	Coarse-grained sandstone	Massive	Greenish when fresh; locally conglomeratic with siltstone and quartz pebbles		
FA3	Mudstone	Massive; laminated	White silky mudstone	Deep marine; below wave-level	Suspended load
	Black shale	Fissility	0.5 to 1.5% TOC		Suspended load and organic productivity
	Siltstone	Laminated	Pale yellow; reddish when rich in iron oxi-hydroxide minerals.		Suspended load and tractive currents
	Rhythmite	Laminated	Silt to mud		
FA4	Sandy-siltstone	Bedded; Hummocky	Greenish when fresh; dolomitic to the top	Shallow to mid-marine; above wave-level	Storm-weather waves and tractive currents
	Siltstone	Laminated	Greenish		
	Dolostone	Massive; layered; low-angle cross stratification; small-scale wave ripples	$\delta^{13}\text{C} = +7.1$ to $+9.6\text{‰}$ $\delta^{18}\text{O} = -6.9$ to $-5.2\text{‰}$		Precipitation; Fair-weather waves; Bedload transport



1

2 Fig. 4: A - Stratigraphic sections and paleogeographic interpretation of the three studied areas of the  
 3 Carrancas Formation. The datum for all sections is the base of the Sete Lagoas Formation. See text  
 4 for stratigraphic details. Not in horizontal scale. B – Detail of the transition from mudstones and  
 5 siltstones (FA3) to dolomitic sandy-siltstones and dolomites (FA4), along with C isotopic profile of  
 6 the reddish dolomite layers. FA: Facies Association (Table 1).

1  
2  
3  
4  
5  
6  
7  
8  
9  
10  
11  
12  
13  
14  
15  
16  
17  
18  
19  
20  
21  
22  
23  
24  
25  
26  
27  
28  
29

#### 4.1.2. Inhaúma area

The Carrancas Formation overlies Archean/Paleoproterozoic gneisses of the Belo Horizonte complex near the cities of Inhaúma and Sete Lagoas (Fig. 2 and 4). The outcrop area is limited to a few square kilometers with 5 meters of clast-supported conglomerate (FA1) capped directly by ~20 m of grey and white siltstone and mudstone (FA3), which is in turn overlain by bedded limestones of the Sete Lagoas Formation. The conglomerate contains exclusively pebble-sized, angular to sub-rounded, gneiss and granite clasts embedded in a quartz-feldspar sandy matrix (Fig. 5). The nearly monolithic clast assemblage and feldspatic matrix suggest a local source area for the Inhaúma conglomerates.

#### 4.1.3. BR-040 area

In the BR-040 area (Fig. 2 and 4), the Carrancas Formation onlaps Archean/Paleoproterozoic gneisses of the Belo Horizonte complex and is predominantly composed of mudstones with intercalations of ferruginous siltstones and black shales (FA3; Table 1). Black shales are much more common here than any other area. Locally, thin (~20 cm) diamictite beds containing granules to small pebble-sized clasts occur within the mudstones. Five meters of well bedded Sete Lagoas Formation limestones featuring low-angle cross stratification occur above a sharp contact with the Carrancas Formation.

### 4.2. Depositional setting of the Carrancas Formation

Stratigraphic and sedimentological data acquired from the three different areas provide a basis for establishing a simple depositional framework for the Carrancas Formation. The lower Carrancas Formations consists of poorly organized gravitationally deposited sediments localized along fault scarps, with alluvial fan conglomerates and diamictites passing upward and laterally into conglomeratic to fine-grained sandstones deposited in fan channels by hyperconcentrated flows, which are best represented in the Pitangui area (Fig. 4). These two facies associations (FA1 and FA2; Table 1) represent a phase of continental rift phase and graben filling.

The upward transition to finer-grained sediments, including mudstones, black shales and ferruginous siltstones, marks an abrupt transgression which flooded local basement highs and

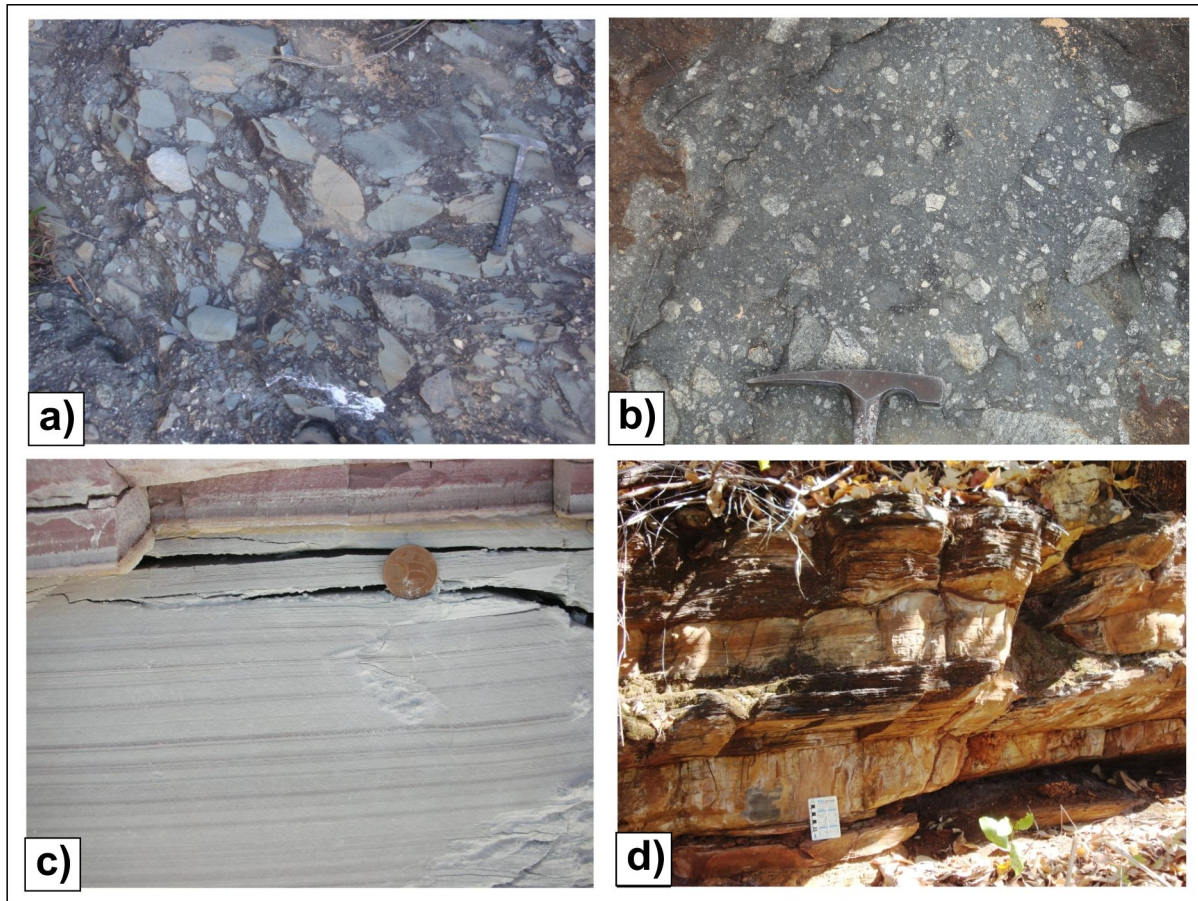
1 resulted in onlap and draping of the previously established topography, in response to active phase of  
2 rifting and high rates of subsidence (Fig. 4). FA3 is the only facies association that occur in all areas  
3 and has sedimentary facies not common in any other Bambui Group unit, thus it is an efficient  
4 marker unit for correlation between areas and clearly marks an important transgressive surface  
5 during Carrancas Formation deposition.

6 Sedimentation rates then outpaced subsidence rates, resulting in an upward-shallowing  
7 succession and occurrence of shallow marine facies and gradual increase in carbonate content.  
8 Symmetrical ripples and small-scale (30 cm high) tabular cross beds in the uppermost dolarenites  
9 imply deposition in a shallow, fair-weather wave setting with episodic currents (Fig. 4).

10 In both the Inhaúma and BR-040 areas, the Carrancas Formation is found in contact with  
11 Paleoproterozoic (ca. 2.2 Ga) amphibolite and metadiabase dykes. According to Chaves and Neves  
12 (2005), dyke emplacement (the Paraopeba swarm) and deformation took place inside vertical  
13 transcurrent shear zones developed during the Paleoproterozoic ( $2.0\pm 0.2$  Ga) orogeny. Later  
14 reactivation of these transcurrent shear zones into brittle normal faults is suggested by the cataclastic  
15 and strongly fractured nature of the dykes, indicating minor extension of the São Francisco crust  
16 (Chaves and Neves, 2005). We suggest that this extensional event may be related to deposition of the  
17 Carrancas Formation. Furthermore, a syn-rift model for the Carrancas Formation is corroborated by  
18 other data. First, the basal conglomerates and diamictites comprise locally derived clasts. Second, the  
19 highly variable thickness of stratigraphic units and facies, including thickening of conglomerates  
20 near inferred basement highs and pinch-out into basement lows, suggests development of horsts and  
21 grabens.

22 The Carrancas Formation onlaps the basement in all areas and its conglomerates were  
23 deposited inside grabens adjacent to rift shoulders, with distal fan channels deposition, suspended  
24 load settling, and bedload transport influenced by storm- to fair-weather waves and episodic bottom  
25 currents, during a single transgressive-regressive sequence. The limited thickness of the Carrancas  
26 Formation (< 80 m) and its highly localized preservation suggest that this extensional event was  
27 minor and maybe restricted to the southern São Francisco craton.

28



1

2 Fig. 5: Lithotypes of the Carrancas Formation in studied areas. (a) Clast-supported conglomerate  
 3 with angular to sub-angular quartzite clasts; (b) Clast-supported conglomerate composed exclusively  
 4 of gneissic and granitic clasts. (c) Ferruginous siltstone lamina and layers intercalated within white  
 5 mudstone; (d) Bedded and finely laminated reddish dolostone.

6

### 4.3. Sedimentary provenance

7

#### 4.3.1. Trace and rare earth elements of Carrancas Formation lithotypes

8

Ten samples of the Carrancas Formation were analyzed for trace and rare earth elements.

9

Four samples were collected in the BR-040 areas, and six are from the Pitangui area (Table 2).

10

The chondrite-normalized REE (Rare Earth Element) data (Boynnton, 1984 – Fig. 6a) show a  
 11 similar pattern for almost all samples, with moderate enrichment of the light rare earth elements  
 12 (LREEs) in comparison with the heavy rare earth elements (HREEs), as quantified by the chondrite-  
 13 normalized ratio of  $La_n/Yb_n$  (1.3-11.3). The samples also show a consistent negative Eu anomaly  
 14 ( $Eu/Eu^*=0.43$  to  $0.75$ ). Samples OP-12 and OP-01 are less REE-enriched, with  $\Sigma REE$  of 35.6 and  
 15 51.6 ppm, respectively. In contrast, the remaining samples show  $\Sigma REE$  of 127.4–293.2 ppm. The  
 16 REE+Y data were normalized to the Post-Archean Australian Shale composition (PAAS from Taylor  
 17 and McLennan, 1985) and show a roughly flat pattern for all samples (Fig. 6b), except for samples

1 OP01 and OP12. Samples from the BR-040 area are more REE+Y enriched then samples from the  
 2 Pitangui area.

3 Table 2: Major and trace elements of the Carrancas Formation in Pitangui and BR-040 areas. BS:  
 4 black shale; FS: ferruginous siltstone; Silt: siltstone; FSand: Fine-grained sandstone; CSC: clast-  
 5 supported conglomerate (matrix).

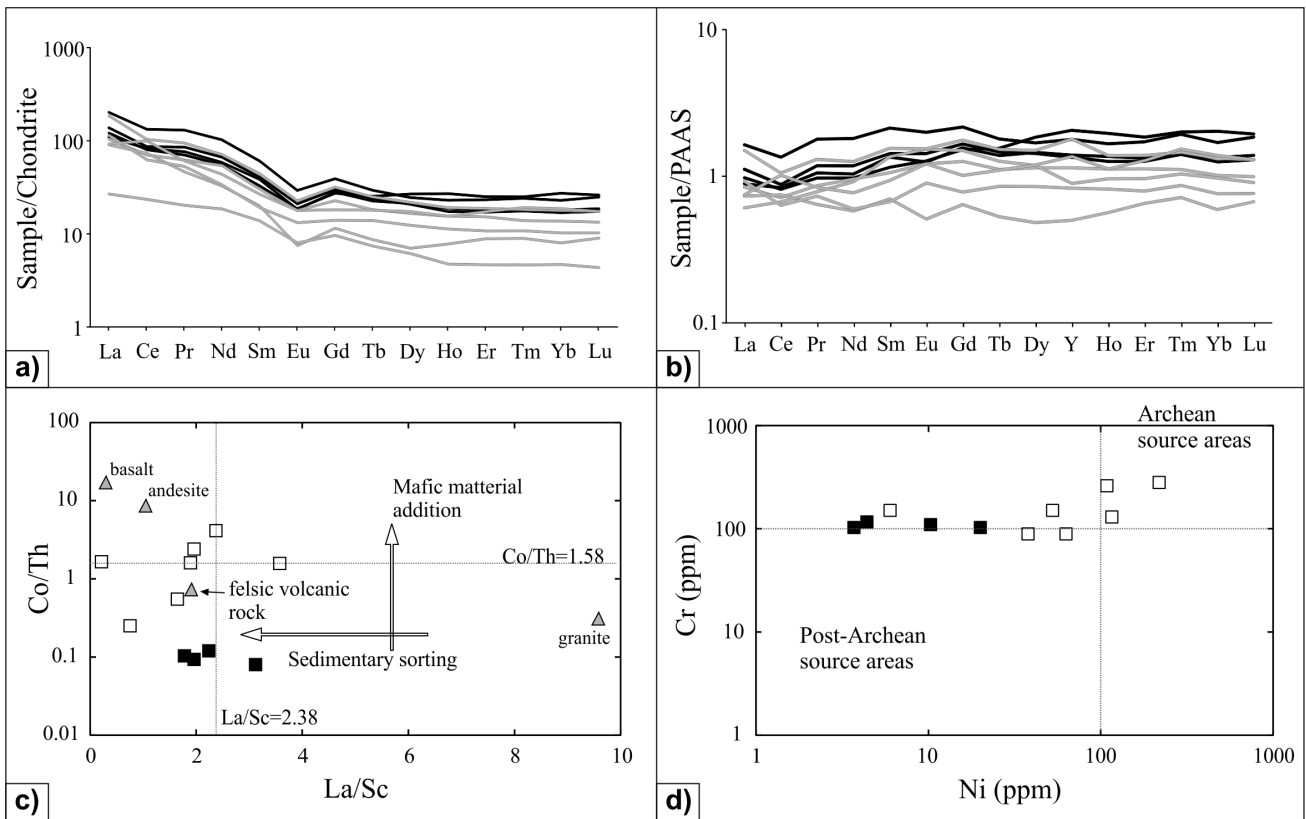
Sample	P05 B	P05 M	P 16	P 02	OP 99	OP 100	OP 01	OP 07	OP 171	OP 188
Facies	BS	BS	Silt	FS	Silt	Silt	FS	FSand	FSand	CSC
Area	BR-040	BR-040	BR-040	BR-040	Pitangui	Pitangui	Pitangui	Pitangui	Pitangui	Pitangui
Cr (ppm)	102.6	102.6	109.4	116.3	88.9	150.5	150.5	280.4	88.9	259.9
Y	37.6	48.1	36.3	55.5	30.8	13.5	8.6	22.4	48.3	36.7
Th	14.5	13.8	15.1	15.1	8.9	10.2	6	9.7	12.7	6.5
Ni	20	3.7	10.3	4.4	37.9	52.6	6	218.6	62.9	108.6
Sc	19	20	19	19	17	17	11	18	16	12
Co	1.5	1.1	1.8	1.4	14.2	5.6	1.5	23.3	19.9	26.8
La	33.9	62.5	42.6	37.3	32.2	28	8.3	35.3	57.2	28.5
Ce	66.5	107.3	69.8	64.7	56.8	59.4	19	50.4	83.6	80.7
Pr	9.3	15.83	10.41	8.57	7.6	5.66	2.47	6.46	11.52	7.4
Nd	35.1	61.3	39.9	32.9	32.4	19.6	11.1	20.2	42.6	26.1
Sm	7.5	11.81	7.91	6.38	5.86	3.89	2.69	3.72	8.61	5.19
Eu	1.35	2.15	1.54	1.37	1.31	0.55	0.59	0.97	1.66	1.31
Gd	7.27	10.09	7.71	7.07	5.87	2.98	2.49	3.63	8.21	4.71
Tb	1.07	1.39	1.13	1.2	0.86	0.41	0.35	0.66	1.18	0.85
Dy	6.81	7.9	6.69	8.63	5.34	2.26	1.98	3.98	7.01	5.59
Ho	1.35	1.65	1.25	1.94	1.11	0.56	0.34	0.81	1.37	1.11
Er	3.78	4.89	3.59	5.26	3.2	1.86	0.98	2.26	3.95	3.64
Tm	0.58	0.78	0.57	0.81	0.45	0.29	0.15	0.35	0.59	0.62
Yb	3.78	4.78	3.53	5.71	2.86	1.67	0.98	2.14	3.74	3.91
Lu	0.6	0.8	0.56	0.84	0.43	0.29	0.14	0.33	0.56	0.56

6

7 A plot of Co/Th vs. La/Sc distinguishes the Pitangui shales as having relatively high Co/Th  
 8 ratios and low La/Sc ratios, consistent a contribution of mafic provenance to these shales (Fig. 6c).  
 9 The Al<sub>2</sub>O<sub>3</sub>/TiO<sub>2</sub> ratios of the investigated shales range from 20 to 21 for the BR-040 area (average  
 10 20.7) and 13 to 27 for the Pitangui area (average 17.7). Based on the work of Girty *et al.* (1996),  
 11 these ranges imply that fine-grained sediments were derived predominantly from intermediate  
 12 igneous rocks, but with some degree of mafic addition, especially in the Pitangui area.

1 The medium to high contents of Cr (88–288, average = 143 ppm) and Ni (4–218, average =  
 2 58 ppm) in the studied shales are consistent with a component of mafic and ultramafic provenance.  
 3 During the Archean the concentration of these elements was higher than in Post-Archean-type rocks.  
 4 (e.g.: Condie, 1993). Hence, Taylor and McLennan (1985) correlate the higher concentrations of Cr  
 5 and Ni in some sedimentary rocks with Archean provenances and use these concentrations to  
 6 discriminate between Archean and post-Archean source areas (Fig. 6d). The higher contents of Cr  
 7 and Ni in shales from the PTA compared to the BRTA is probably due to the erosion of mafic-  
 8 ultramafic rocks in the meta-volcano-sedimentary Archean Rio das Velhas Supergroup basement,  
 9 which is found only in the Pitangui area.

10 Distinct whole rock geochemical data between the different areas is consistent with variable  
 11 compositions from local sources areas and limited mixing of sediments derived from these local  
 12 sources.



13  
 14 Fig. 6: REE data normalized to chondrite (a), from Boynton (1984) and PAAS (b) from McLennan  
 15 (1989). Grey lines – Pitangui area; Black lines – BR-040 area; (c) La/Sc vs. Co/Th. The dotted lines  
 16 represent PAAS values (Taylor and McLennan 1985); (d) Ni–Cr binary diagram. Archean and Post-  
 17 Archean fields from Taylor and McLennan (1985). White squares – Pitangui area; black squares –  
 18 BR-040 area.

19 4.3.2. Sm-Nd data constraints on source area

1 The results for the Sm-Nd data are presented in Table 3. Initial isotope ratios were calculated  
 2 at 660 Ma, as an approximation of a pre-Marinoan age. The fine-grained lithotypes from the  
 3 Carrancas Formation fall into two groups based on their  $T_{DM}$  model ages and  $\epsilon Nd_{(660Ma)}$ : one with  
 4 model ages ranging from 1.7 to 2.1 Ga and  $\epsilon Nd_{(660Ma)}$  between -5.9 to -7.8; and another group with  
 5 older  $T_{DM}$  (2.8-3.0 Ga) and more evolved  $\epsilon Nd_{(660Ma)}$  (-17.7 to -21.6).

7 Table 3: Sm and Nd isotope data from Carrancas Formation.  $T_{DM}$  model ages were calculated  
 8 following Goldstein *et al.* (1984). BS: black shale; FS: ferruginous siltstone; Silt: siltstone; CSC:  
 9 clast-supported conglomerate (matrix).  $T_{DM}$  was not calculated for samples with very high  
 10  $^{147}Sm/^{144}Nd$ .

Sample ID	Rock	Nd (ppm)	Sm (ppm)	$^{147}Sm/^{144}Nd$	$^{143}Nd/^{144}Nd \pm 2\sigma$	$\epsilon Nd_{(0)}$	$\epsilon Nd_{(660 Ma)}$	$T_{DM}$	$f(Sm/Nd)$
<i>BR-040 Area</i>									
P-05-G	BS	60.3	11.9	0.1194	$0.511895 \pm 09$	-14.5	-7.8	2.03	-0.39
OP5-7.5	BS	50.0	11.3	0.1365	$0.511904 \pm 09$	-14.3	-9.1	2.5	-0.31
OP5-4.5	BS	31.8	7.9	0.1499	$0.511950 \pm 14$	-13.4	-9.4	-	-0.24
OP5-3	BS	45.2	11.1	0.1489	$0.511974 \pm 14$	-12.9	-8.8	-	-0.24
BS - 4	BS	29.0	7.9	0.1650	$0.511976 \pm 12$	-12.9	-10.2	-	-0.16
BS-2	BS	34.9	8.9	0.1555	$0.511954 \pm 16$	-13.3	-9.8	-	-0.21
P-16	Silt	46.2	9.1	0.1201	$0.511945 \pm 08$	-13.5	-6.9	1.96	-0.39
P-02	FS	13.9	2.9	0.1290	$0.511968 \pm 13$	-13.1	-7.2	2.12	-0.34
<i>Pitangui Area</i>									
OP-100	Silt	19.9	3.6	0.1094	$0.511144 \pm 08$	-29.1	-21.6	2.92	-0.44
OP-99	Silt	22.2	4.6	0.1251	$0.511412 \pm 08$	-23.9	-17.7	2.98	-0.36
OP-88	CSC	40.3	7.8	0.1177	$0.511358 \pm 09$	-25.0	-18.1	2.83	-0.40
OP-49A	Silt	67.5	12.5	0.1121	$0.511956 \pm 09$	-13.3	-5.9	1.79	-0.43
OP-171	Silt	63.4	10.9	0.1043	$0.511895 \pm 10$	-14.5	-6.5	1.75	-0.47
OP-01	FS	6.83	1.71	0.1518	$0.512060 \pm 10$	-11.3	-7.4	-	-0.23

11  
 12 Post-depositional fractionation of Sm/Nd can result in higher  $^{147}Sm/^{144}Nd$  ratios and hence  
 13 higher  $T_{DM}$  model ages. However, the  $^{147}Sm/^{144}Nd$  ratios for the three samples with higher  $T_{DM}$  ages  
 14 are consistent with average crustal values (Goldstein *et al.*, 1984) suggesting that these Nd model  
 15 ages are reliable (Table 3). On the other hand, some of the black shales and sample OP-01 have  
 16 anomalously high  $^{147}Sm/^{144}Nd$  ratios, rendering the model age for these samples suspect.

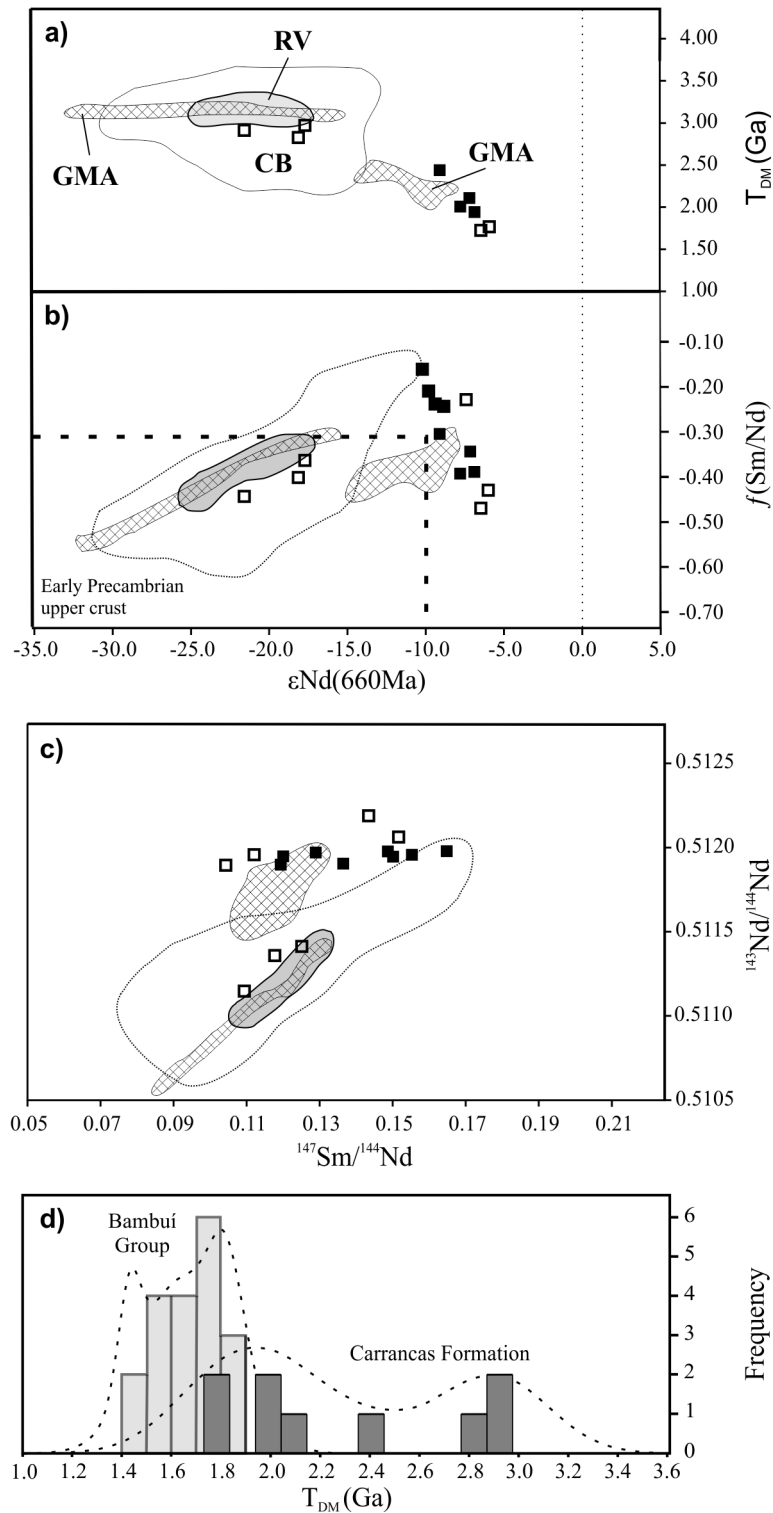
17 The Nd isotope compositions of the Pitangui and BR-040 areas share similar patterns, except  
 18 for three samples of the Pitangui area (Fig. 7). Excluding the three samples with different isotopic  
 19 signals, the samples of the two studied areas overlap to some degree, suggesting similar source areas  
 20 for the fine-grained rocks in both areas. In the diagrams of Fig. 7 these samples are outliers of the

1 most probable source areas fields, which are inferred to be the Archean Rio das Velhas Supergroup  
2 (RV; David, 2011) and the Archean-Paleoproterozoic granite-gneiss cratonic basement (CB; Noce *et*  
3 *al.*, 2000). Mixing of these two proposed sources along with a third source rock with a younger Nd  
4 isotope signature must be considered. A similar scenario has been inferred for fine-grained rocks in  
5 the upper Bambuí Group (e.g. Rodrigues, 2008; Pimentel *et al.*, 2011). Although a source area with  
6 such a young Nd isotope signature is not present in the southern basement of the São Francisco  
7 Craton (Teixeira *et al.*, 1996, 2000; Noce *et al.*, 2000), it is quite common in the Brasília fold belt, on  
8 the western margin of the Bambuí Group (e.g.: Pimentel *et al.*, 2000, 2001).

9 It is well established that the Brasília fold belt was one of the main source areas to the  
10 Bambuí basin. For comparison, the diagram in Figure 8 presents one additional possible source area  
11 for the sediments of the Carrancas Formation: the early to middle volcanic sequences of the  
12 Neoproterozoic Goiás Magmatic Arc (ca. 900-750 Ma) (GMA; Pimentel *et al.*, 2000). These plots  
13 suggest a relationship between the Sm-Nd data from the Carrancas Formation and the probable  
14 mixing between these three proposed source areas. Specific source areas for outlier samples remain  
15 unclear. We suggest that the southern basement of the São Francisco craton, with significant  
16 additions of younger arc-related rocks from the Brasília fold belt, make up the main sediment source  
17 for the fine-grained rocks of the Carrancas Formation. The isotopic composition represents the  
18 variable mixing of these two composite end-members.

19 The three other samples with older Nd model ages and more negative  $\epsilon\text{Nd}_{(660\text{Ma})}$  values plot  
20 within the granite-gneiss CB and near the Rio das Velhas Supergroup (RV) fields and clearly show a  
21 different provenance than the other samples (Fig. 7). For these samples, a single local provenance is  
22 more logical, as implied by the high proportion of local, angular clasts in the nearby breccias. Hence,  
23 in contrast with the majority of the shales from the Carrancas Formation, the source sediment of  
24 these three samples was exclusively derived from Archean-Paleoproterozoic southern basement of  
25 the São Francisco Craton. Similarly, two black shales from the BR-040 area also share older  $T_{\text{DM}}$   
26 ages (2.0 and 2.5 Ga), but with less evolved  $\epsilon\text{Nd}_{(660\text{Ma})}$  (-7.8 and -9.1).

27 Fig. 7d compares Nd model ages of the Carrancas Formation with data from the Bambuí  
28 Group (Pimentel *et al.* 2001). The Bambuí Group shows a narrower, younger, and more continuous  
29 range in Nd model ages than the Carrancas Formation. Thus, the sediments comprising the Carrancas  
30 Formation were heterogeneously sourced. This is consistent with stratigraphic and lithochemical  
31 data, and the polymodal data suggest that these sources may have been widely separated and that the  
32 sediments did not have the chance to become fully mixed on their way to the Carrancas sedimentary  
33 basins.



1

2 Fig. 7: Comparative plots of Nd isotopic characteristics of fine-grained rocks of the Carrancas  
 3 Formation and frequency histogram of Nd model ages. A, B, C) Pitangui area: white squares; BR-  
 4 040 area: black squares. The limiting fields represent possible source areas: CB – granite-gneiss  
 5 cratonic basement (Noce *et al.*, 2000); RV – Rio das Velhas Supergroup (David, 2011); GMA –  
 6 Goías Magmatic Arc (Pimentel *et al.*, 2000). Early Precambrian upper crust field from McLennan  
 7 and Hemming (1992). D) Frequency histogram and probability curve of Nd model ages for the Bambuí Group lithotypes (from Pimentel *et al.*,  
 8 2001), and Nd model ages for the Carrancas Formation in Pitangui and BR-040 areas.  
 9

### 4.3.3. Zircon U-Pb data

A total of 53 zircon grains were extracted from a sandstone sample in the Pitangui area and analyzed by LA-ICP-MS, but only a subset of 26 zircons that showed low discordance (< 10%) and low common lead abundances are considered here. Results are displayed in Fig. 8.

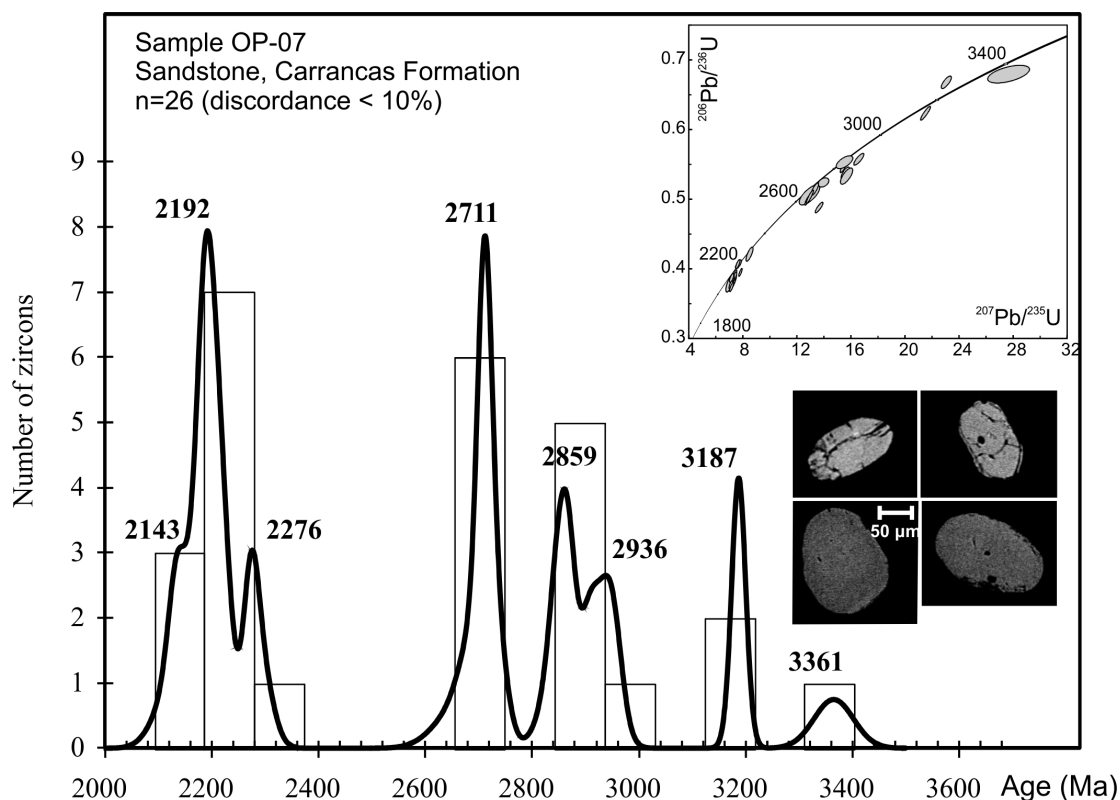


Fig. 8: Frequency histogram, probability curve and concordia diagram of ages obtained from U-Pb (LA-ICP-MS) analyzes on detrital zircon grains extracted from a sandstone sample of the Carrancas Formation, and scanning electron microscope (SEM) images for some analyzed grains.

The probability density plot encloses 3 main peaks, at 2192, 2711 and 3187 Ma. These data suggest source rocks for the Carrancas Formation within the following ages: 42% Rhyacian ( $2204 \pm 11$  Ma); 23% Neoproterozoic ( $2712 \pm 14$  Ma); and two Mesoproterozoic peaks of  $2887 \pm 15$  Ma (23%); and  $3198 \pm 18$  Ma (12%).

The bulk of the São Francisco craton is made up of Archean terranes (3.4–2.5 Ga) that coalesced during the Rhyacian orogens (2.2–2.0 Ga; Teixeira *et al.*, 1996; Teixeira *et al.*, 2000; Noce *et al.*, 2000). Thus, the local cratonic basement may have sourced the entire zircon population.

The Archean zircon ages spectra of the Carrancas Formation reflect three main events that affected the southern crust of the São Francisco Craton during the Archean. The ca. 3360 and 3190 Ma peaks relate to the U-Pb ages from the crustal generation that may have continued until ca. 2.9–

1 3.0 Ga (Noce *et al.*, 1998). The ca. 2940 and 2860 Ma peaks may represent late stage crustal addition  
2 and migmatization events that reworked the protoliths. Finally, the ca. 2710 Ma peak is consistent  
3 with reworking and granitic magmatism, which occurred until ca. 2.6 Ga, when the cratonic crust  
4 stabilized (e.g. Noce *et al.*, 1998; Teixeira *et al.*, 2000). Another potential source of the Archean  
5 zircons is reworked metasedimentary rocks of the ca. 2.6–2.5 Ga Rio das Velhas Supergroup, which  
6 surround the Carrancas Formation outcrops in the PTA.

7 The Paleoproterozoic U-Pb zircon ages from the Carrancas Formation define two main peaks  
8 of ca. 2280 and 2190 Ma, consistent with the pre- to syn-collisional evolution of the  
9 Paleoproterozoic Mineiro belt. This orogenic belt rims the southernmost margin of the São Francisco  
10 Craton, from the Quadrilátero Ferrífero westward (Fig. 2) and is composed of gneisses, granitoids,  
11 supracrustal sequences, greenstone belts and mafic dykes that were deformed and metamorphosed at  
12 2.1–1.9 Ga (e.g.: Teixeira *et al.*, 2000, 2008).

13 The U-Pb data include now Mesoproterozoic or Neoproterozoic ages to corroborate the  
14 hypothesis of younger source areas based on the Sm-Nd data. In the case of the Carrancas Formation,  
15 except for the three northern samples in the PTA with older Nd model ages, all others show Nd  
16 model ages younger than the youngest U-Pb age. There are two possible explanations for this  
17 geochronological discrepancy. One is that the U-Pb spectra, like the Sm-Nd data, are variable  
18 between sites. A second possibility is local confinement of heavy minerals by placer deposition. Sm  
19 and Nd in sediments are concentrated mainly in fine-grained minerals, especially the clay mineral  
20 fraction. Clay minerals travel long distances more efficiently than heavy minerals, such as zircon,  
21 garnet, monazite, spinel and rutile, which are hydraulically fractionated during transport (Morton and  
22 Hallsworth, 1999). The Sm-Nd isotope data suggest contributions from Proterozoic sources,  
23 probably located within the Brasília fold belt to the west. As the Carrancas Formation is located on  
24 the opposite margin of the basin and was deposited during initiation of the Bambuí basin, the  
25 sediment transport systems could have impeded transport of heavy minerals, which were trapped in  
26 placer deposits prior to entering the Bambuí basin, whereas younger Nd and Sm signals preserved in  
27 clays covered large distances.

#### 28 **4.1. Carbon and oxygen isotopes: correlations and temporal implications**

29 The reddish dolostone of the Pitangui area and sixteen dolomitic clasts from a conglomerate  
30 of the same area were measured for  $\delta^{13}\text{C}$  and  $\delta^{18}\text{O}$  compositions. A thin interval of laminated  
31 limestones which overlap the Carrancas Formation in the BR-040 area was also analyzed for C, O  
32 isotopes. All data are presented in Table 4.

1 Carbon ( $\delta^{13}\text{C}$ ) and oxygen ( $\delta^{18}\text{O}$ ) isotope compositions of the reddish dolostone range from  
 2 +7.1 to +9.6‰ and -5.2 to -6.9‰, respectively. The carbonate clasts are all pebble-sized, massive  
 3 dolomitic clasts that are scattered through a clast-supported conglomerate and yield heavy  $\delta^{13}\text{C}$   
 4 compositions (+3.6 to +9.4‰). The thin preserved limestones on top of the Carrancas Formation in  
 5 the BR-040 area show almost constant values in  $\delta^{13}\text{C}$  (0.68-0.76‰) and  $\delta^{18}\text{O}$  (-8.68 to -8.62‰).

6 Table 4:  $\delta^{13}\text{C}$  and  $\delta^{18}\text{O}$  compositions along with elemental data of carbonate clasts and layers from  
 7 the Carrancas Formation and Sete Lagoas Formation in studied areas.

Sample	$\delta^{13}\text{C}_{(\text{VPDB})}$	$\delta^{18}\text{O}_{(\text{VPDB})}$	Mg/Ca	Mn/Sr
Reddish dolostone layers				
Carrancas Formation – Pitangui area				
OP100-0	8.7	-6.2		
OP100-0.5	8.5	-6.4	0.64	16.9
OP100-1	8.6	-6.9		
OP100-1.5	9.2	-6.6	0.65	7.6
OP100-2	9.3	-6.5		
OP100-2.5	8.6	-6.7	0.65	15.9
OP100-3	9.0	-6.7		
OP100-3.5	9.3	-6.4	0.61	9
OP100-4.5	9.3	-6.6		
OP100-5	7.1	-5.3	0.64	6.2
OP100-6	8.6	-6.2		
OP100-7	9.1	-6.6	0.68	23.1
OP100-8	8.2	-5.4		
OP100-8.5	9.5	-6.5	0.63	12.5
OP100-9.5	9.4	-6.5		
OP100-10	9.6	-5.2	0.62	10.6
OP100-10.5	9.4	-6.7		
OP100-11	8.3	-6.3	0.71	10.5
OP100-11.5	8.5	-6.1		
OP100-12	9.3	-6.9	0.61	7.9
OP100-12.5	9.5	-6.6		
OP100-13.5	9.5	-6.5	0.62	8.3

Carbonate clasts  
Carrancas Formation – Pitangui area

CAR-C1	4.79	-6.51	0.51	24.3
CAR-C2	7.71	-8.82	0.53	12.6
CAR-C3	9.23	-7.19	0.52	8.8
CAR-C4	8.99	-6.66	0.54	22.8
CAR-C5	9.18	-6.64	0.54	10.2
CAR-C6	6.73	-7.46	0.52	26.3
CAR-C7	3.6	-7.86	0.48	41.5
CAR-C8	9.15	-7.03	0.52	16.5
CAR-C9	7.53	-11.45	0.5	24.5
CAR-C10	9.11	-6.38	0.51	34
CAR-C11	9.38	-7.31	0.53	9.4
CAR-C12	8.99	-6.9	0.54	29.6
CAR-C13	8.42	-7.26	0.54	7.2
CAR-C14	3.88	-5.93	0.52	30.3
CAR-C15	4.15	-10.7	0.55	43.5
CAR-C16	8.44	-8.51	0.52	14.3

Limestone layers  
Sete Lagoas Formation – BR-040 area

SL-0	0.68	-8.68	0.01	0.7
SL-1	0.69	-8.87	0.01	0.8
SL-2	0.73	-8.79	0.03	0.6
SL-2.5	0.74	-8.73		
SL-3	0.73	-8.76	0.01	0.4
SL-3.5	0.77	-8.6		
SL-4	0.76	-8.62	0.01	0.7

1

2

3

4

5

---

The reddish dolostones occur only in the upper part of the Carrancas Formation in the Pitangui area and display strongly positive  $\delta^{13}\text{C}$  values, up to +9.6‰ (Fig. 4B). Carbon-isotopic compositions higher than +5‰ in the Bambuí Group are restricted to the middle/upper Sete Lagoas

1 Formation and throughout the Lagoa do Jacaré Formation (e.g.: Iyer *et al.*, 1995; Santos *et al.*, 2004;  
2 Alvarenga *et al.*, 2007, 2014; Paula-Santos *et al.*, 2015), which are mainly calcitic and dark-gray to  
3 black organic-rich limestones, unlike the reddish dolomites. These are the first strongly positive  $\delta^{13}\text{C}$   
4 data obtained from the lower Bambuí Group. Because these rocks pre-date the Sete Lagoas  
5 Formation and are not obviously glaciogenic, they must be pre-Marinoan in age. High  $\delta^{13}\text{C}$   
6 carbonates occur both during the Tonian and Cryogenian interglacial interval (Kaufman *et al.*, 1997;  
7 Halverson *et al.*, 2005). Although we cannot rule out the possibility that these  $^{13}\text{C}$ -enriched  
8 Carrancas dolostones are earlier Neoproterozoic in age, the most parsimonious interpretation is that  
9 they are Cryogenian and correspond to the 'Keele Peak'. This peak in  $\delta^{13}\text{C}$  values from +8 to +10‰  
10 is well documented globally (e.g. Kaufman *et al.*, 1997; McKirdy *et al.*, 2001; Halverson *et al.*,  
11 2005; Johnston *et al.*, 2012) and is followed by the Trezona negative carbon isotope anomaly, which  
12 shortly precedes the onset of Marinoan glaciation (Halverson *et al.*, 2002).

13 In the Araçuaí fold belt, to the northeast, the so-called Tijucuçu sequences comprises an ~200  
14 m-thick mixed siliciclastic-carbonate transgressive sequence tract deposited in a rift to passive  
15 margin basin, representing fluvial plain to shallow shelf deposits (Fraga, 2013) (Fig. 1). The  
16 Tijucuçu sequence unconformably overlies the Duas Barras and Domingas formations and is itself  
17 unconformably overlain by continental and marine glacial diamictites of the Serra do Catuni  
18 Formation. All of these units belong to the Cryogenian Macaúbas Group (Pedrosa-Soares *et al.*,  
19 2011; Babinski *et al.*, 2012; Fraga, 2013). Fraga *et al.* (2014) analyzed C, O isotopes on calcareous  
20 layers of the upper 40 m of the Tijucuçu sequence and obtained almost constant values of  $\delta^{13}\text{C}$   
21 around +10‰ with a sharp decrease to -1.0‰ towards the top. These isotopic values are consistent  
22 with the  $\delta^{13}\text{C}$  Keele peak followed by the initial decline into the Trezona negative carbon isotope  
23 anomaly, implying a pre-Marinoan (ca. 635 Ma) age for the Tijucuçu sequence and a late  
24 Cryogenian pre-glacial record on the eastern margin of the São Francisco craton.

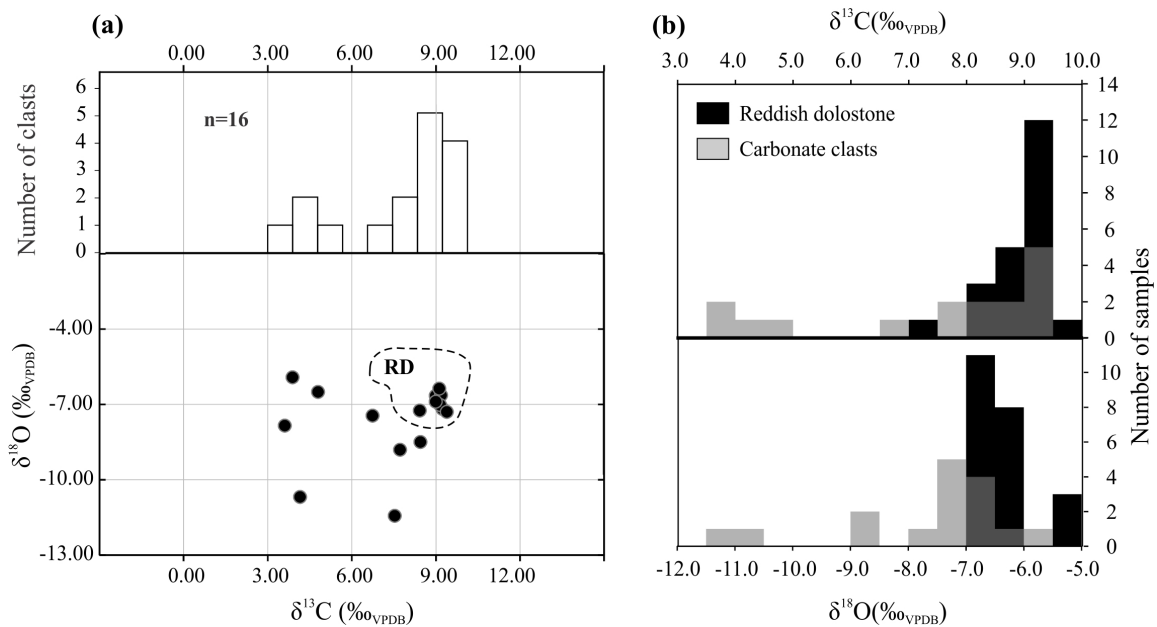
25 It is widely believed that the glaciogenic Serra do Catuni Formation in the Araçuaí fold belt  
26 correlates with the Jequitaiá Formation on the craton (Karfunkel and Hoppe, 1988; Uhlein *et al.*,  
27 1998, 1999; Martins-Neto *et al.*, 2001). Thus, we propose a similar correlation between the pre-  
28 glacial Tijucuçu sequence and Carrancas Formation, in which the continental extension on the  
29 southern São Francisco crust may be a minor expression of the rifting at the eastern margin, and  
30 suggest that both of these units capture the Keele Peak, and hence represent the Cryogenian  
31 interglacial interval.

32 The histogram in Fig. 9a shows a bimodal distribution for the  $\delta^{13}\text{C}$  compositions of the  
33 dolomitic clasts in Carrancas Formation conglomerates in the Pitangui area, with a prominent peak at  
34 9.1‰ and four values clustering around 4‰. This isotopic distribution suggests two different

1 carbonate sources. Carbon and oxygen isotope variations are shown in Fig. 9a with a number of  
 2 samples clustered around  $\delta^{13}\text{C}$  and  $\delta^{18}\text{O}$  of +9‰ and -7‰, respectively. The  $\delta^{13}\text{C}$  and  $\delta^{18}\text{O}$  data of  
 3 the carbonate clasts in the Pitangui area are effectively identical to the reddish dolostone layers and  
 4 imply an intraformational provenance for clast-supported conglomerate in the Pitangui Area (Fig. 9a  
 5 and 9b).

6 Considering that the conglomerate is stratigraphically below the reddish dolostones, another  
 7 source area with high  $\delta^{13}\text{C}$  must be found. This suggests that there were carbonates depositing  
 8 locally prior to the Keele Peak (dolostone clasts with less positive  $\delta^{13}\text{C}$  values), and that the Keele  
 9 peak may be represented by more than just the high  $\delta^{13}\text{C}$  reddish dolostones; i.e. there was tectonism  
 10 and cannibalization (clast-supported conglomerate deposition) at this time on the southern São  
 11 Francisco craton and only the end of the Keele Peak is preserved in the Carrancas Formation.

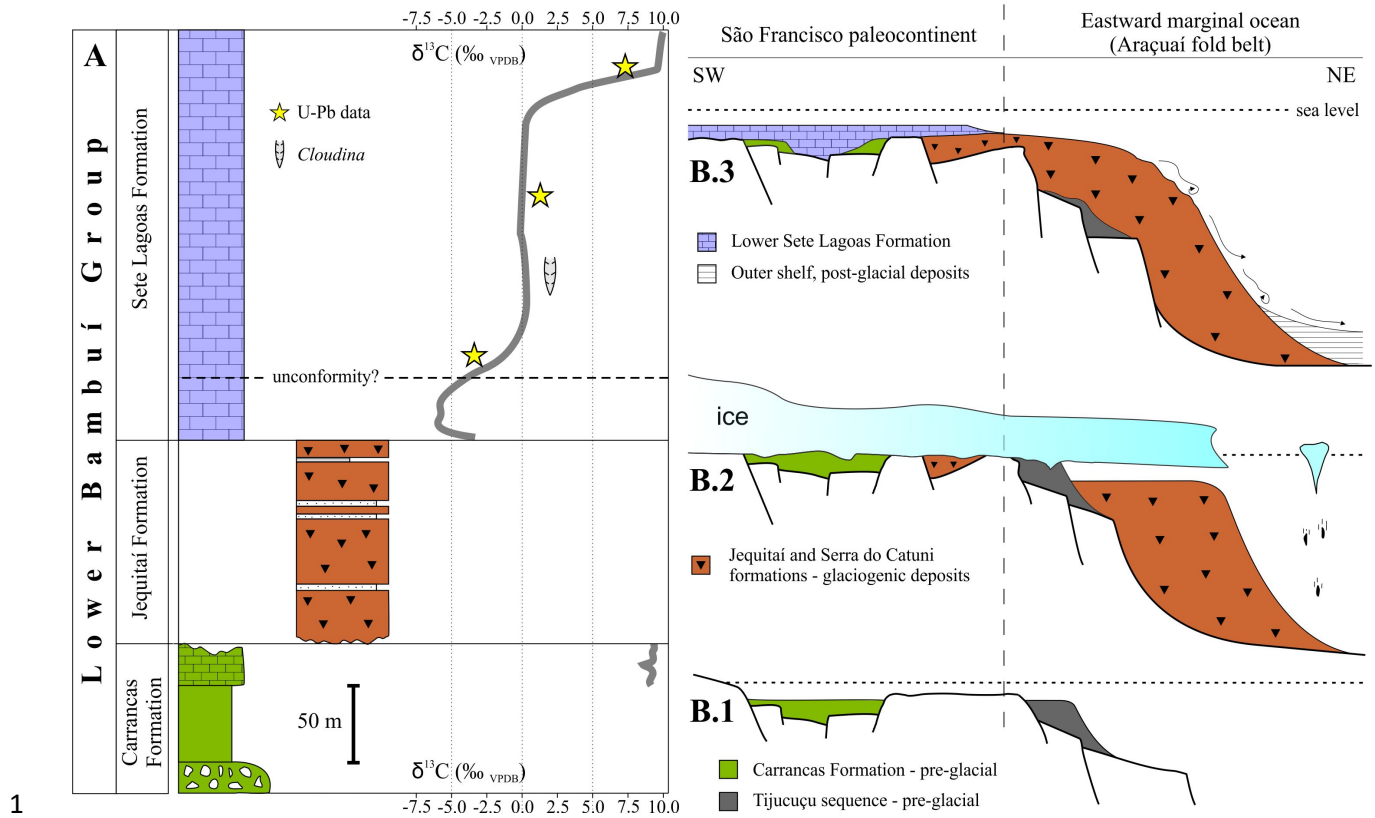
12 Above the mudstones of the Carrancas Formation in the BR-040 area, a thin interval of  
 13 laminated limestones is preserved. The C and O isotopic compositions are near constant, ranging  
 14 from 0.68 to 0.76‰ for  $\delta^{13}\text{C}$  and -8.68 to -8.62‰ for  $\delta^{18}\text{O}$ . We suggest that this limestone represent  
 15 the Sete Lagoas Formation and thus display a direct contact between pre- and post-glacial sections.  
 16 This stratigraphic relation is seen in other outcrops of the Carrancas Formation, as occurrences of the  
 17 glaciogenic Jequitai Formation are missing in the southern Bambuí basin.



18  
 19 Fig. 9: (a) Histogram and  $\delta^{13}\text{C}$  vs  $\delta^{18}\text{O}$  crossplot of carbonate clasts from the Pitangui area. RD:  
 20 isotopic compositional field of the reddish dolostone (b) Histogram of  $\delta^{13}\text{C}$  and  $\delta^{18}\text{O}$  distribution of  
 21 carbonate clasts compared to reddish dolostone layers.

22 **5. CONCLUSIONS**

1           Stratigraphic and isotopic data presented in this paper suggest sedimentation of the Carrancas  
2 Formation inside small continental rift basins that opened on the southern São Francisco  
3 paleocontinent prior to the onset of the end-Cryogenian (Marinoan) glaciation. Basal conglomerates  
4 pass upward and laterally into turbidites, which are in turn overlain by mudstones, siltstones and  
5 black shales deposited during a basin-wide transgression. Reddish dolostones and dolarenites locally  
6 occur at the top of the Carrancas Formation. All Facies Associations are recorded in the Pitangui  
7 area; however, FA2 and FA4 are missing in the BR-040 and Inhaúma areas. Mudstones and  
8 siltstones of FA3 are the main lithocorrelation interval and their first appearance marks a  
9 transgressive surface over uplifted basement blocks and intercommunication between previously  
10 isolated grabens. Conglomerates, consisting of intrabasinal clasts within the Carrancas Formation  
11 (FA1) are interpreted as gravity flow deposits controlled by faulted basin margins. No evidence for  
12 glacial influence is present in the Carrancas Formation. Sm-Nd and lithochemical data corroborate  
13 deposition within partially connected sub-basins and with a source of poorly-mixed sediments. A  
14 well-defined trend of positive  $\delta^{13}\text{C}$  values (+7 to +9‰) for the reddish dolostone beds occur in the  
15 upper Carrancas Formation in the Pitangui area, beneath basal Ediacaran cap carbonates of the Sete  
16 Lagoas Formation. These anomalous high positive values are identical to those observed during the  
17 Cryogenian interglacial Keele peak, and prior to the Trezona negative carbon isotope excursion  
18 (Halverson *et al.*, 2005). Another pre-glacial succession in the Araçuaí fold belt to the east – the  
19 Tijucuçu sequence – shares similar C isotopic compositions with the Carrancas Formation (high  $\delta^{13}\text{C}$   
20 values). We interpret these two units to be correlative, implying a more widespread pre-Marinoan  
21 record on the São Francisco craton and surrounding fold belt (Fig. 10).



1  
 2 Fig. 10: A) Composite stratigraphic column for the lower Bambuí Group and its  $\delta^{13}\text{C}$  isotopic  
 3 profile, from pre- to post-glacial units. Approximate stratigraphic locations of *Cloudina* occurrences  
 4 and U-Pb data are based on facies associations and  $\delta^{13}\text{C}$  compositions (Warren *et al.*, 2014; Paula-  
 5 Santos *et al.*, 2015). An unconformity separates the late-Cryogenian to earliest Ediacaran, lower  
 6 intracratonic sequence, from the late Ediacaran, foreland-basin deposits. B.1, B.2, B.3 show The  
 7 Cryogenian to basal Ediacaran evolution of the southeast São Francisco crust and its eastern margin,  
 8 interpreted in terms of three phases: B.1 — Cryogenian interglacial interval. Deposition of the  
 9 Carrancas Formation inside grabens on the São Francisco crust, and, to the northeast, the Tijucuçu  
 10 sequence developed over a rift to passive margin basin. B.2 — Onset of the end-Cryogenian  
 11 glaciation is marked by localized deposition of the Jequitai Formation in fault-controlled basement  
 12 lows on the paleocontinent. Its counterpart, the Serra do Catuni Formation, filled a deeper basin to  
 13 the east with sediment derived predominantly from subglacial meltwater plumes. Basement and pre-  
 14 glacial units were intensely eroded by glacial abrasion. B.3 — End of the late Cryogenian  
 15 (Marinoan) glaciation and deposition of the Sete Lagoas cap carbonate on a shallow shelf. Further  
 16 east, reworked glacial sediments with sparse calcareous lenses were deposited at the same time.

17 We propose a new interpretation for the lower Bambuí Group and southern São Francisco  
 18 paleocontinent that is consistent with the isotopic and stratigraphic data presented in this paper (Fig.  
 19 10). The Carrancas Formation was deposited during the Cryogenian interglacial interval in partially  
 20 connected grabens or half-grabens that were like produced by a minor, short term, rifting event over  
 21 the southern São Francisco craton (Fig. 4 and Fig. 10-B.1). At the same time on the eastern margin of  
 22 the craton, the Tijucuçu sequence was deposited within a continental rift that evolved into a passive  
 23 margin basin. A shallowing upward top and the occurrence of dolostones with high  $\delta^{13}\text{C}$  composition

1 in the Carrancas Formation highlights a base-level fall that may have heralded the onset of  
2 glaciation. At this time, a continental to marine glacial environment occupied much of the São  
3 Francisco paleocontinent and its margins (Fig. 10-B.2). The Jequitai Formation was deposited in an  
4 epicontinental sea that flooded the craton, while its counterpart, the Serra do Catuni Formation, filled  
5 the passive margin basin at the eastward marginal ocean. Subglacial gravity flows and dropstones  
6 from the breakup of the ice shelf are identified throughout the Serra do Catuni and others formations  
7 in the Araçuaí fold belt (Karfunkel & Hoppe, 1998; Pedrosa-Soares *et al.*, 2011) (Fig. 10-B.2). Both  
8 glaciogenic units share almost identical  $\delta^{13}\text{C}$  (0 to -7‰) and  $\delta^{18}\text{O}$  (-7 to -15‰) values for their  
9 carbonate clasts, including a few clasts with positive  $\delta^{13}\text{C}$  as high as +7‰ (Caxito *et al.*, 2012 and  
10 references there in). Thus, erosion of a pre-glacial carbonate platform with mainly negative  $\delta^{13}\text{C}$   
11 values was suggested by Caxito *et al.* (2012). The Carrancas Formation and the Tijucuçu sequence  
12 are likely candidates for the source of  $^{13}\text{C}$ -enriched carbonate clasts within the glacial diamictites,  
13 while the older Domingas Formation and the upper Tijucuçu sequence carbonates may be the source  
14 for carbonate clasts with negative  $\delta^{13}\text{C}$  composition (Santos *et al.* 2004; Caxito *et al.*, 2012). Sub-  
15 glacial erosion and post-glacial rebound may also have reinforced the patchy preservation pattern of  
16 the Carrancas Formation. Cap carbonate of the lower Sete Lagoas Formation deposited immediately  
17 in the aftermath of the end-Cryogenian glaciation filled an irregular relief, likely accentuated by  
18 glacial erosion and glacio-isostatic rebound along the shoreline (Fig. 10-B.3) (Vieira *et al.*, 2007a,  
19 2015). A foreslope equivalent of the post-glacial carbonate platform developed over an outer shelf  
20 environment to the east, represented by reworked glacial sediments and intercalated carbonate lenses  
21 (Fig. 10-B.3).

22 The Jequitai Formation does not occur in the southern Bambuí basin, probably due to the  
23 presence of the Sete Lagoas paleo-high, which may have hindered the preservation of glaciogenic  
24 sediments. The thickest and best exposed occurrences of the Jequitai Formation are located away  
25 from these paleo-highs (e.g.: Cuckov *et al.*, 2005; Uhlein *et al.*, 2011b). Although debate persists  
26 over the depositional age of the Jequitai Formation and the entire Bambuí Group, stratigraphic and  
27 isotopic data from the lowermost Bambuí are consistent with a late-Cryogenian to earliest Ediacaran  
28 age. Indeed, the Bambuí Group appears to span the entirely end-Cryogenian (Marinoan) glaciation  
29 event and the post-glacial transgression. To the extent that the middle to upper Bambuí Group is late  
30 Ediacaran, as implied by fossil and zircon data, this suggests an unconformity in the middle of the  
31 Sete Lagoas Formation carbonates, separating a lower end-Cryogenian to earliest Ediacaran basin,  
32 from a middle to late Ediacaran basin (Fig. 10A).

## 33 6. ACKNOWLEDGMENTS

1 This paper is part of continuous work on the Bambuí Group headed by the Neoproterozoic  
2 research group of the Universidade Federal de Minas Gerais, Brazil. GJU was supported by research  
3 grant from CNPq and by the ELAP (Emerging Leaders in the Americas Program) of the Canadian  
4 Bureau for International Education/Foreign Affairs and International Trade Canada, during his stay  
5 at the GEOTOP Research Center, Montréal, Canada. AU is supported by CNPq (447449/2014-1) and  
6 FAPEMIG grants (APQ-01711-14). GPH's involvement in this project was supported by an NSERC  
7 Discovery grant. FAC is supported by FAPEMIG grants APQ-00914-14 and PPM-00539-15. GMC  
8 was supported by a NSERC Vanier Fellowship.

## 9 7. REFERENCES

- 10 ALKMIM, F.F. (2004) O que faz de um cráton um cráton? O Cráton do São Francisco e as  
11 revelações almeidianas ao delimitá-lo. In: *Geologia do Continente Sul-Americano: evolução*  
12 *da obra de Fernando Flávio Marques de Almeida* (Ed. by V. Mantesso-Neto, A. Bartorelli, C.  
13 D. R. Carneiro & B. B. Brito-Neves), pp. 17-35. Beca, São Paulo.
- 14 ALKMIM, F.F. & MARSHAK S. (1998). Transamazonian Orogeny in the Southern São Francisco  
15 Craton Region, Minas Gerais, Brazil: evidence for Paleoproterozoic collision and collapse in  
16 the Quadrilátero Ferrífero. *Precambrian Research*, 90, 29-58
- 17 ALKMIM, F.F. & MARTINS-NETO, M.A. (2001) A bacia intracratônica do São Francisco:  
18 arcabouço estrutural e cenários evolutivos. In: *A Bacia do São Francisco. Geologia e recursos*  
19 *naturais* (Ed. by C. P. Pinto & M. A. Martins-Neto), pp. 9-30. SBG, Belo Horizonte.
- 20 ALLEN, P.A. & HOFFMAN, P.F. (2005) Extreme winds and waves in the aftermath of a  
21 Neoproterozoic glaciation. *Nature*, 433, 123-127.
- 22 ALMEIDA, F.F.M. (1977) O Cráton do São Francisco. *Revista Brasileira de Geociências*, 7, 349-  
23 364.
- 24 ALVARENGA, C.J.S., GIUSTINA, M.E.S.D, SILVA, N.G.C., SANTOS, R.V., GIOIA, S.M.C.L.,  
25 GUIMARÃES E.M., DARDENNE, M.A., SIAL, A.N., FERREIRA V.P. (2007) Variações  
26 dos isótopos de C e Sr em carbonatos pré e pós-glaciação Jequitai (Esturtiano) na região de  
27 Bezerra-Formosa, Goiás. *Revista Brasileira de Geociências*, 37(4), 147-155.
- 28 ALVARENGA, C.J.S., SANTOS, R.V., VIEIRA, L.C., LIMA, B.A.F., MANCINI L.H. (2014)  
29 Meso-Neoproterozoic isotope stratigraphy on carbonates platforms in the Brasília Belt of  
30 Brazil. *Precambrian Research*, 251, 164-180.
- 31 BABINSKI, M., PEDROSA-SOARES, A.C., TRINDADE, R.I.F., MARTINS, M., NOCE, C.M.,  
32 LIU, D. (2012) Neoproterozoic glacial deposits from the Araçuaí orogen, Brazil: age,  
33 provenance and correlations with the São Francisco craton and West Congo belt. *Gondwana*  
34 *Research*, 21, 451-465.
- 35 BABINSKI, M., VIEIRA, L.C. & TRINDADE, R.I.F. (2007) Direct dating of the Sete Lagoas cap  
36 carbonate (Bambuí Group, Brazil) and implications for the Neoproterozoic glacial events.  
37 *Terra Nova*, 19, 401-406.
- 38 BOYNTON, W.V. (1984) Cosmochemistry of the rare earth elements: meteorite studies. In: *Rare*  
39 *Earth Element Geochemistry* (Ed. by P. Henderson), pp. 63-114. Elsevier, Amsterdam.
- 40 BÜHN, B., PIMENTEL, M.M., MATTEINI, M. & DANTAS, E.L. (2009) High spatial resolution  
41 analysis of Pb and U isotopes for geochronology by laser ablation multi-collector inductively  
42 coupled plasma mass spectrometry (LA-MC-IC-MS). *Anais da Academia Brasileira de*  
43 *Ciências*, 81, 1-16.

- 1 CAXITO, F.A., HALVERSON, G.P., UHLEIN, A., STEVENSON, R., DIAS, T.G. & UHLEIN,  
2 G.J. (2012) Marinoan glaciation in east central Brazil. *Precambrian Research*, 200-203, 38-  
3 58.
- 4 CHAVES, A.O., NEVES J.M.C. (2005) Radiometric ages, aeromagnetic expression, and general  
5 geology of mafic dykes from southeastern Brazil and implications for African–South  
6 American correlations. *Journal of South American Earth Sciences*, 19, 387-397.
- 7 CONDIE, K.C. (1993) Chemical composition and evolution of the upper continental crust:  
8 contrasting results from surface samples and shales. *Chemical Geology* 104, 1-37.
- 9 CUKROV, N., ALVARENGA, C.J.S., UHLEIN, A. (2005) Litofácies da glaciação neoproterozoica  
10 nas porções sul do cráton do São Francisco: Exemplos de Jequitai (MG) e Cristalina (GO).  
11 *Revista Brasileira de Geociências*, 35(1), 69–76.
- 12 DARDENNE, M.A. (1978) Síntese sobre a estratigrafia do Grupo Bambuí no Brasil Central. 30°  
13 Congresso Brasileiro de Geologia. 2, 597-610.
- 14 DAVID, M.E.V. (2011) Estudo termocronológico e evolução metalogenética da mineralização  
15 aurífera do Depósito Turmalina – MG. PhD Thesis, USP, Instituto de Geociências, 142p.
- 16 EVANS, D.A.D. (2000) Stratigraphic, geochronological, and paleomagnetic constraints upon the  
17 Neoproterozoic climatic paradox. *American Journal of Science*, 300, 347-433.
- 18 EYLES, N. & JANUSZCZAK, N. (2004) ‘Zipper-rift’: a tectonic model for Neoproterozoic  
19 glaciations during the breakup of Rodinia after 750 Ma. *Earth-Science Reviews*, 65, 1-73.
- 20 FRAGA, L.M.S. (2013) Análise estratigráfica do Grupo Macaúbas no domínio meridional da Serra  
21 do Espinhaço, Minas Gerais. PhD Thesis, UFMG, IGC, 189p.
- 22 FRAGA, L.M.S., NEVES, S.C., UHLEIN, A., SIAL, A.N., PIMENTEL, M.M., HORN A.H. (2014)  
23 C-, Sr-isotope stratigraphy of carbonate rocks from the Southern Espinhaço Ridge, Minas  
24 Gerais, southeastern Brazil. *Anais da Academia Brasileira de Ciências*, 86, 633-648.
- 25 FONT, E., NÉDÉLEC, A., TRINDADE, R.I.F. & MOREAU, C. (2010) Fast or slow melting of the  
26 Marinoan snowball Earth? The cap dolostone record. *Palaeogeography, Palaeoclimatology,*  
27 *Palaeoecology*, 295, 215-225.
- 28 GIRTY, G.H., RIDGE, D.L., KNAACK, C., JOHNSON, D. & AL-RIYAMI, R.K. (1996)  
29 Provenance and depositional setting of Paleozoic chert and argillite, Sierra Nevada,  
30 California. *Journal of Sedimentary Research*, 66, 107-118.
- 31 GOLDSTEIN, S.L., ONIONS, R.K., HAMILTON, P.J. (1984) A Sm-Nd isotopic study of  
32 atmospheric dusts and particulates from major river systems. *Earth and Planetary Science*  
33 *Letters*, 70, 221-236.
- 34 GONÇALVES, L., ALKMIM, F.F., PEDROSA-SOARES, A.C., DUSSIN, I.A., VALERIANO,  
35 C.M., LANA, C., TEDESCHI, M. (2015) Granites of the intracontinental termination of a  
36 magmatic arc: an example from the Ediacaran Araçuaí orogen, southeastern Brazil.  
37 *Gondwana Research*, <http://dx.doi.org/10.1016/j.gr.2015.07.015>
- 38 GUIRRA, A.P.M., REIS, H.L.S., SUSS, J., ALKMIM, F.F. (2014) A porção basal do Grupo Bambuí  
39 na região de Pompéu (MG): Levantamento estratigráfico preliminar baseado em dados de  
40 poço. In: Congresso Brasileiro de Geologia, 47, Anais, vol.1
- 41 HALVERSON, G.P., HOFFMAN, P.F., SCHRAG, D.P., KAUFMAN, A.J. (2002) A major  
42 perturbation of the carbon cycle before the Ghaub glaciation (Neoproterozoic) in Namibia:  
43 Prelude to snowball Earth? *Geochemistry, Geophysics, Geosystems*, 3, 16p.
- 44 HALVERSON, G.P., HOFFMAN, P.F., SCHRAG, D.P., MALOOF, A.C., RICE, A.H.N. (2005).  
45 Toward a Neoproterozoic composite carbon-isotope record. *GSA Bulletin*, 117, 1181-1207.
- 46 HALVERSON, G.P., MALOOF, A.C. & HOFFMAN, P.F. (2004) The Marinoan glaciation  
47 (Neoproterozoic) in northeast Svalbard. *Basin Research*, 16, 297-324.
- 48 HOFFMAN, P.F. (2011) Strange bedfellows: glacial diamictite and cap carbonate from the Marinoan  
49 (635 Ma) glaciation in Namibia. *Sedimentology*, 58, 57-119.

- 1 HOFFMAN, P.F. & HALVERSON, G.P. (2008) Otavi Group of the western Northern Platform, the  
2 Eastern Kaoko Zone and the western Northern Margin Zone. In: *The Geology of Namibia*  
3 (Ed. by R. M. Miller), pp. 69-136. Geological Survey of Namibia, Windhoek.
- 4 HOFFMAN, P.F., HALVERSON, G.P., DOMACK, E.W., HUSSON, J.M., HIGGINS, J.A. &  
5 SCHRAG, D.P. (2007) Are basal Ediacaran (635 Ma) post-glacial “cap dolostones”  
6 diachronous? *Earth and Planetary Science Letters*, 258, 114-131.
- 7 HOFFMAN, P.F. & LI, Z.-X. (2009) A palaeogeographic context for Neoproterozoic glaciation.  
8 *Palaeogeography, Palaeoclimatology, Palaeoecology*, 277, 158-172.
- 9 HOFFMAN, P.F. & SCHRAG, D.P. (2002) The snowball Earth hypothesis: testing the limits of  
10 global change. *Terra Nova*, 14, 129-155.
- 11 ISOTTA, C.A.L., ROCHA-CAMPOS, A.C., YOSHIDA, R. (1969) Striated pavement of the Upper  
12 Precambrian glaciation in Brazil. *Nature*, 222, 466–468.
- 13 IYER, S.S., BABINSKI M., KROUSE H.R., CHEMALE Jr., F. (1995) Highly <sup>13</sup>C-enriched  
14 carbonate and organic matter in the Neoproterozoic sediments of the Bambuí Group, Brazil.  
15 *Precambrian Research*, 73, 271-282.
- 16 JAMES, N.P., NARBONNE, G.M., KYSER, T.K. (2001). Late Neoproterozoic cap carbonates:  
17 Mackenzie Mountains, northwestern Canada: Precipitation and global glacial meltdown.  
18 *Canadian Journal of Earth Sciences*, 38, 1229–1262.
- 19 JOHNSTON, D.T., MACDONALD, F.A., GILL, B.C., HOFFMAN, P.F., SCHRAG, D.P. (2012)  
20 Uncovering the Neoproterozoic carbon cycle, *Nature*, 483, 320-323.
- 21 KARFUNKEL, J. & HOPPE, A. (1988) Late Precambrian glaciation in central-eastern Brazil:  
22 synthesis and model. *Palaeogeography Palaeoclimatology Palaeoecology*, 65, 1–21.
- 23 KAUFMAN, A.J., KNOLL, A.H., NARBONNE, G.M. (1997) Isotopes, ice ages, and terminal  
24 Proterozoic earth history: Proceedings of the National Academy of Sciences of the United  
25 States of America, 94, 6600–6605.
- 26 KENNEDY, M.J. & CHRISTIE-BLICK, N. (2011) A condensation origin for Neoproterozoic cap  
27 carbonates. *Geology*, 39, 319-322.
- 28 LAMB, M.P., FISCHER, W.W., RAUB, T.D., PERRON, J.T., MYROW, P.M. (2012) Origin of  
29 giant wave ripples in snowball Earth cap carbonate. *Geology*, 40, 827–830.
- 30 LUDWIG, K.R. (2008) User's manual for Isoplot 3.6. A geochronological toolkit for Microsoft  
31 Excel. Special Publication, No. 4, Berkeley Geochronologic Center. Berkeley, USA.
- 32 MARTINS, M. & LEMOS, V.B. (2007) Análise estratigráfica das seqüências neoproterozóicas da  
33 Bacia do São Francisco. *Revista Brasileira de Geociências*, 37, 156-167.
- 34 MARTINS-FERREIRA, M.A.C., CAMPOS, J.E.G., ALVARENGA, C.J.S. (2013). A Formação  
35 Jequitai na região de Vila Boa, GO: exemplo de sedimentação por geleiras terminais no  
36 Neoproterozóico. *Brazilian Journal of Geology*, 43(2), 373-384.
- 37 MARTINS-NETO, M.A., PEDROSA-SOARES, A.C., LIMA S.A.A. (2001) Tectono-sedimentary  
38 evolution of sedimentary basins from late Paleoproterozoic to late Neoproterozoic in the São  
39 Francisco Craton and Araçuaí fold belt, eastern Brazil. *Sedimentary Geology*, 141-142, 343-  
40 370.
- 41 MCKIRDY, D.M., BURGESS, J.M., LEMON, N.M., YU, X., COOPER, A.M., GOSTIN, V.A.,  
42 JENKINS, R.J.F., BOTH, R.A. (2001) A chemostratigraphic overview of the late Cryogenian  
43 interglacial sequence in the Adelaide Fold-Thrust Belt, South Australia. *Precambrian*  
44 *Research*, 106, 149–186.
- 45 MCLENNAN, S.M. (1989) Rare earth elements in sedimentary rocks: influence of provenance and  
46 sedimentary processes. . In: *Geochemistry and Mineralogy of the Rare Earth Elements* (Ed.  
47 by B. Lipin & G. McKay), pp. 169-200. Mineralogical Society of America.
- 48 MCLENNAN, S.M. & HEMMING S. (1992) Samarium/neodymium elemental and isotopic  
49 systematics in sedimentary rocks. *Geochimica e Cosmochimica Acta*, 56, 887-898.

- 1 MORTON, A.C. & HALLSWORTH, C.R. (1999) Processes controlling the composition of heavy  
2 mineral assemblages in sandstones. *Sedimentary Geology*, 124, 3-29.
- 3 NOCE, C.M., MACHADO, N. & TEIXEIRA, W. (1998) U-Pb geochronology of gneisses and  
4 granitoids in the Quadrilátero Ferrífero (southern São Francisco craton): age constraints for  
5 Archean and Paleoproterozoic magmatism and metamorphism. *Revista Brasileira de*  
6 *Geociências*, 28, 95-102.
- 7 NOCE, C.M., TEIXEIRA, W., QUÉMÉNEUR, J.J.G., MARTINS, V.T.S. & BOLZACHINI, E.  
8 (2000) Isotopic signatures of Paleoproterozoic granitoids from the southern São Francisco  
9 Craton and implications for the evolution of the Transamazonian Orogeny. *Journal of South*  
10 *American Earth Sciences*, 13, 225-239.
- 11 PAULA-SANTOS, G.M., BABINSKI, M., KUCHENBECKER, M., CAETANO-FILHO, S.,  
12 TRINDADE, R.I.F. & PEDROSA-SOARES, A.C. (2015) New evidence of an Ediacaran age  
13 for the Bambuí Group in southern São Francisco craton (eastern Brazil) from zircon U-Pb  
14 data and isotope chemostratigraphy. *Gondwana Research*, 18, 1-19.
- 15 PEDROSA-SOARES, A.C., BABINSKI, M., NOCE, C.M., MARTINS, M.S., QUEIROGA, G. &  
16 VILELA, F. (2011) The Neoproterozoic Macaúbas Group (Araçuaí orogen, SE Brazil) with  
17 emphasis on the diamictite formations. In: *The Geological Record of Neoproterozoic*  
18 *Glaciations* (Ed. by E. Arnaud, G. P. Halverson & G. Shields), *Memoir 36*, pp. 523-534.  
19 *Geological Society of London, London.*
- 20 PEDROSA-SOARES, A.C., NOCE, C.M., WIEDEMANN, C.M., PINTO, C.P. (2001) The Araçuaí-  
21 West Congo orogen in Brazil: An overview of a confined orogen formed during  
22 Gondwanland assembly. *Precambrian Research*, 110, 307-323.
- 23 PIMENTEL, M.M., DARDENNE, M.A., FUCK, R.A., VIANA, M.G., JUNGES, S.L., FISCHER,  
24 D.P., SEER, H.J. & DANTAS, E.L. (2001) Nd isotopes and the provenance of detrital  
25 sediments of the Neoproterozoic Brasília Belt, central Brazil. *Journal of South American*  
26 *Earth Sciences*, 14, 571-585.
- 27 PIMENTEL, M.M., FUCK, R.A. & GIOIA, S.M.C.L. (2000) The Neoproterozoic Goiás magmatic  
28 arc, central Brazil: A review and new Sm-Nd isotopic data. *Revista Brasileira de Geociências*,  
29 30, 35-39.
- 30 PIMENTEL, M.M., RODRIGUES, J.B., DELLAGIUSTINA, M.E.S., JUNGES, S., MATTEINI, M.  
31 & ARMSTRONG, R. (2011) The tectonic evolution of the Neoproterozoic Brasília Belt,  
32 central Brazil, based on SHRIMP and LA-ICPMS U-Pb sedimentary provenance data: A  
33 review. *Journal of South American Earth Sciences*, 31, 345-357.
- 34 PIN, C. & ZALDUEGUI, J.F.S. (1997) Sequential separation of light rare-earth elements, thorium,  
35 and uranium by miniaturized extraction chromatography: application to isotopic analyses of  
36 silicate rocks. *Analytica Chimica Acta*, 339, 79-89.
- 37 REIS, H.L.S., ALKMIM, F.F. (2015) Anatomy of a basin-controlled foreland fold-thrust belt curve:  
38 the Três Marias salient, São Francisco basin, Brazil. *Marine and Petroleum Geology*,  
39 <http://dx.doi.org/10.1016/j.marpetgeo.2015.07.013>
- 40 RIBEIRO, J.H., TULLER, M.P., PINHO, J.M.M., SIGNORELLI, N., FÉBOLI, W.L. (2008) A  
41 fácies diamictito da Formação Carrancas, Grupo Bambuí, na região sudoeste da bacia do São  
42 Francisco, Minas Gerais. In: *Congresso Brasileiro de Geologia*, 44, Anais, p.913.
- 43 ROCHA-CAMPOS, A.C., YOUNG, G.M., SANTOS, P.R. (1996) Re-examination of a striated  
44 pavement near Jequitaiá, MG: implications for proterozoic stratigraphy and glacial geology.  
45 *Anais da Academia Brasileira de Ciências*, 68(4), 593.
- 46 RODRIGUES, J.B. (2008) Proveniência de sedimentos dos grupos Canastra, Ibiá, Vazante e Bambuí  
47 – um estudo de zircões detríticos e idades modelo Sm-Nd. PhD Thesis, UnB, IG, 128p.
- 48 ROMANO, A.W. (2007) Nota explicativa da Folha Pará de Minas (SE.23-Z-C-IV) 1:100.000.  
49 Convênio CPRM-UFMG, 65p.

- 1 ROMANO, A.W. & KNAUER, L.G. (2003) Evidências da glaciação neoproterozoica na base do  
2 Grupo Bambuí - região de Onça do Pitangui - Minas Gerais. In: Simpósio de Geologia de  
3 Minas Gerais, 12, Anais, v. 1
- 4 SANTOS, R.V., ALVARENGA, C.J.S., BABINSKI, M., RAMOS, M.L.S., CUKROV, N.,  
5 FONSECA, M.A., SIAL, A.N., DARDENNE, M.A., NOCE, C.M. (2004) Carbon isotopes of  
6 Mesoproterozoic–Neoproterozoic sequences from Southern São Francisco craton and Araçuaí  
7 Belt, Brazil: Paleographic implications. *Journal of South American Earth Sciences*, 18, 27-39.
- 8 SANTOS, T.R. (2012). Químioestratigrafia das rochas carbonáticas da Formação Sete Lagoas:  
9 Grupo Bambuí – Arcos, MG. MSc. Dissertation, UFPR, 132p.
- 10 SGARBI, G.N.C., TULLER, M.P.; RIBEIRO, J.H., MARTINS-NETO M.A. (2003) The Carrancas  
11 Facies and the Sete Lagoas Formation: the record of the Neoproterozoic Snowball Earth  
12 glaciation in the Bambuí Group, São Francisco Basin. In: Simpósio de Geologia de Minas  
13 Gerais, 12, Anais, p.30.
- 14 SHIELDS, G.A. (2005) Neoproterozoic cap carbonates: a critical appraisal of existing models and  
15 the plumeworld hypothesis. *Terra Nova*, 17, 299-310.
- 16 SIAL, A.N., DARDENNE, M.A., MISI, A., PEDREIRA, A.J., GAUCHER, C., FERREIRA, V.P.,  
17 SILVA-FILHO, M.A., UHLEIN, A., PEDROSA-SOARES, A.C., SANTOS, R.V., EGYDIO-  
18 SILVA, M., BABINSKI, M., ALVARENGA, C.J.S., FAIRCHILD, T.R. & PIMENTEL,  
19 M.M. (2009) The São Francisco Palaeocontinent. In: *Neoproterozoic-Cambrian Tectonics,  
20 Global Change and Evolution: a focus on southwestern Gondwana* (Ed. by C. Gaucher, A. N.  
21 Sial, G. P. Halverson & H. E. Frimmel), *Developments in Precambrian Geology*, 16, pp. 31-  
22 69. Elsevier.
- 23 TAYLOR, S.R. & MCLENNAN, S.M. (1985) *The continental crust. Its composition and evolution.*  
24 Blackwell, Oxford.
- 25 TEIXEIRA, W., ÁVILA, C.A. & NUNES, L.C. (2008) Nd–Sr isotopic geochemistry and U–Pb  
26 geochronology of Fé granitic gneiss and Lajedo granodiorite: implications for  
27 Paleoproterozoic evolution of the Mineiro belt, southern São Francisco Craton. *Geologia USP  
28 Série Científica*, 8, 53-73.
- 29 TEIXEIRA, W., CARNEIRO, M.A., NOCE, C.M., MACHADO, N., SATO, K. & TAYLOR, P.T.  
30 (1996) Pb, Sr and Nd isotope constraints on the Archaean evolution of gneissic-granitoid  
31 complexes in the southern São Francisco Craton, Brazil. *Precambrian Research*, 78, 151-164.
- 32 TEIXEIRA, W., SABATE, P., BARBOSA, J., NOCE, C.M. & CARNEIRO, M.A. (2000) Archean  
33 and Paleoproterozoic Tectonic Evolution of the São Francisco Craton, Brazil. In: *Tectonic  
34 Evolution of South America* (Ed. by U. G. Cordani, E. J. Milani, A. Thomaz-Filho & D. A.  
35 Campos), pp. 101-137. 31st IGC, Rio de Janeiro.
- 36 TRINDADE, R.I.F. & MACOUIN, M. (2007) Palaeolatitude of glacial deposits and  
37 palaeogeography of Neoproterozoic ice ages. *Comptes Rendus Geoscience*, 339, 200-211.
- 38 TULLER, M.P., RIBEIRO, J.H., SIGNORELLI, M., FEBOLI, W.L. & PINHO, J.M.M. (2008)  
39 Proposta de uma nova seção-tipo da Formação Carrancas, Grupo Bambuí, na região de  
40 Inhaúma, Minas Gerais. 44º Congresso Brasileiro de Geologia, 929.
- 41 UHLEIN, A., ALVARENGA, C.J.S., DARDENNE, M.A. & TROMPETTE, R.R. (2011b) The  
42 glaciogenic Jequitáí Formation, southeastern Brazil. In: *The Geological Record of  
43 Neoproterozoic Glaciations* (Ed. by E. Arnaud, G. P. Halverson & G. Shields-Zhou), *Memoir  
44 36*, pp. 51-66. Geological Society of London, London.
- 45 UHLEIN, A., BAPTISTA, M.C., SEER, H.J., CAXITO, F.A., UHLEIN, G.J. & DARDENNE, M.A.  
46 (2011a) A Formação Lagoa Formosa, Grupo Bambuí (MG): sistema deposicional de leque  
47 submarino em bacia de ante-país. *Geonomos*, 19, 163-172.
- 48 UHLEIN, A., TROMPETTE, R.R., ALVARENGA C.J.S. (1999) Neoproterozoic glacial and  
49 gravitational sedimentation on a continental rifted margin: The Jequitáí-Macaúbas sequence  
50 (Minas Gerais, Brazil). *Journal of South American Earth Sciences*, 12, 435-451.

- 1 UHLEIN, A., TROMPETTE, R.R., EGYDIO-SILVA, M. (1998) Proterozoic rifting and closure, SE  
2 border of the São Francisco Craton, Brazil. *Journal of South American Earth Sciences*, 11,  
3 191-203.
- 4 UHLEIN, G.J., CARVALHO, J.F.M.G., UHLEIN, A., CAXITO, F.A., HALVERSON, G.P. &  
5 SIAL, A. (2013) Estratigrafia e Sedimentologia da Formação Carrancas, Grupo Bambuí, nas  
6 regiões de Belo Horizonte e Pitangui, MG. *Geonomos*, 20, 18.
- 7 VALERIANO, C.M., TEIXEIRA, W., HEILBRON, M. & SIMÕES, L.S.A. (2000) Southern  
8 Brasília Belt (SE Brazil): Tectonic discontinuities, K-Ar data and evolution during the  
9 Neoproterozoic Brasileiro Orogeny. *Revista Brasileira de Geociências*, 30, 195-199.
- 10 VIEIRA, L.C., ALMEIDA, R.P., TRINDADE, R.I.F., NOGUEIRA, A.C.R. & JANIKIAN, L.  
11 (2007a) A Formação Sete Lagoas em sua área tipo: fácies, estratigrafia e sistemas  
12 deposicionais. *Revista Brasileira de Geociências*, 37, 1-14.
- 13 VIEIRA, L.C., TRINDADE R.I.F., NOGUEIRA A.C.R., ADER M. (2007b) Identification of a  
14 Sturtian cap carbonate in the Neoproterozoic Sete Lagoas carbonate platform, Bambuí Group,  
15 Brazil. *Comptes Rendus Geoscience*, 339, 240-258.
- 16 VIEIRA, L.C., NÉDÉLEC A., FABRE, S., TRINDADE, R.I.F., ALMEIDA, R.P. (2015) Aragonite  
17 crystal fans in Neoproterozoic cap carbonates: a case study from Brazil and implications for  
18 the post-snowball earth coastal environment. *Journal of Sedimentary Research*, 85, 285-300.
- 19 WARREN, L.V., QUAGLIO, F., RICCOMINI, C., SIMOES, M.G., POIRE, D.G., STRIKIS, N.M.,  
20 ANELLI, L.E. & STRIKIS, P.C. (2014) The puzzle assembled: Ediacaran guide fossil  
21 Cloudina reveals an old proto-Gondwana seaway. *Geology*, 42, 391-394.
- 22 ZALÁN, P.V. & ROMEIRO-SILVA, P.C. (2007) Proposta de mudança significativa na coluna  
23 estratigráfica da Bacia do São Francisco. In: *Simpósio de Geologia do Sudeste*, 10,  
24 Diamantina, SBG-MG, Programação e Livro de Resumos, p. 96.